Spin Equilibria in Monomeric Manganocenes: Solid State Magnetic and EXAFS Studies

*Marc D. Walter, Chadwick D. Sofield, Corwin H. Booth and Richard A. Andersen**

Department of Chemistry and Chemical Sciences Division of Lawrence Berkeley National Laboratory, University of California, Berkeley, California 94720

raandersen@lbl.gov

RECEIVED DATE (to be automatically inserted after your manuscript is accepted if required according to the journal that you are submitting your paper to)

Email: raandersen@lbl.gov

Abstract. Magnetic susceptibility measurements and X-ray data confirm that tert-butyl substituted manganocenes $[(Me_3C)_nC_5H_{5-n}]_2Mn$ (n= 1, 2) follow the trend previously observed with the methylated manganocenes, i.e., electron donating groups attached to the Cp ring stabilize the low-spin (LS) electronic ground state relative to Cp_2Mn and exhibit higher spin-crossover (SCO) temperatures. However, introducing three CMe_3 groups on each ring gives a temperature invariant high-spin (HS) state manganocene. The origin of the high-spin state in $[1,2,4\text{-}(Me_3C)_3C_5H_2]_2Mn$ is due to the significant bulk of the $[1,2,4\text{-}(Me_3C)_3C_5H_2]^-$ ligand, which is sufficient to generate severe inter-ring steric strain that prevents the realization of the low-spin state. Interestingly, the spin transition in $[1,3\text{-}(Me_3C)_2C_5H_3]_2Mn$ is accompanied by a phase transition resulting in a significant irreversible hysteresis (ΔT_c = 16 K). This structural transition was also observed by extended X-ray absorption fine-structure (EXAFS) measurements. Magnetic susceptibility studies and X-ray diffraction data on $SiMe_3$ substituted

manganocenes $[(Me_3Si)_nC_5H_{5-n}]_2Mn$ (n= 1, 2, 3) show high-spin configuration in these cases. Although tetra- and hexasubstituted manganocenes are high-spin at all accessible temperatures, the disubstituted manganocenes exhibit a small low-spin admixture at low temperature. In this respect it behaves similarily to $[(Me_3C)(Me_3Si)C_5H_3]_2Mn$, which has a constant low-spin admixture up to 90 K and then gradually converts to high-spin. Thermal spin-trapping can be observed for $[(Me_3C)(Me_3Si)C_5H_3]_2Mn$ on rapid cooling.

Introduction

The molecular and electronic structure of manganocenes have been of interest since $(C_5H_5)_2Mn$, Cp_2Mn, were first prepared by Wilkinson [1, 2] and Fischer [3] more than fifty years ago. In the solid state, $(C_5H_5)_2Mn$ is a chain polymer quite unlike the typical sandwich structure of D_{5h} and D_{5d} symmetry,[4] although in gas phase Cp_2Mn has a sandwich structure like Cp_2Fe.[5, 6] As originally reported, the magnetic behavior of Cp_2Mn was not readily understood, until its polymeric structure was determined. A plot of the magnetic moment as a function of T shows that the individual Mn(II) centers are antiferromagnetically coupled in the temperature range 90-432 K above which it undergoes an abrupt phase transition to a pink form, where its magnetic moment is consistent with an isolated S= 5/2 paramagnet, i.e. high-spin (HS) Mn(II). When diluted in Cp_2Mg, Cp_2Mn behaves as an isolated S= 5/2 paramagnet from 90 to 500 K. The substituted derivative $(MeC_5H_4)_2Mn$ shows similar behavior in its magnetic susceptibility.[7] The gas phase electron diffraction data of $(MeC_5H_4)_2Mn$ have been interpreted as consisting of two monomeric spin isomers, where the ratio of high-spin (Mn-C(ave)= 2.43 Å) to low-spin (Mn-C(ave)= 2.14 Å) is 60:40 at 100 °C.[8, 9] This gas phase structural study supports the deductions of earlier gas phase photoelectron spectroscopy (PES) studies that $(MeC_5H_4)_2Mn$ is a spin equilibrium molecule in gas phase while Cp_2Mn exists predominantly as the high-spin isomer.[10] The EPR studies of Ammeter and Maki have shown that Cp_2Mn and $(MeC_5H_4)_2Mn$ in frozen solution and doped in a host matrix of Cp_2M or $(MeC_5H_4)_2M$ (M= Mg, Fe), respectively, behave as spin crossover molecules, where

a low-spin (LS) state is stabilized by about 0.5 kcal mol^{-1}.[11-14] The low-spin isomer ($^2E_{2g}$ in D_{5h} symmetry) has a doubly degenerate ground state and behaves as a dynamic Jahn-Teller molecule. The nature of the potential energy surface of the dynamic Jahn-Teller distortion depends upon the substituents on the Cp-ring and the host metallocene, which has lead to the study of various ring substituted compounds. The only other manganocene whose electronic structure has been studied extensively is $(Me_5C_5)_2Mn$.[15-17] The magnetic moment in the solid state (5-100 K) shows it to be low-spin and its EPR spectrum in frozen glasses and solid solutions of $(Me_5C_5)_2Fe$ show that the ground state is $^2E_{2g}$, consistent with the gas phase PES data. The room temperature solid-state X-ray crystal structure of $(Me_5C_5)_2Mn$ with the Mn-C(ave) distances of 2.11 Å show it is low-spin but there are several distortions, which have been ascribed to a static Jahn-Teller distortion.[16] Herein, we report the synthesis, molecular structure and electronic properties of a series of trimethylsilyl and tert-butyl substituted manganocenes.

Results and Discussion

Synthesis. The synthesis of the manganocenes described in this paper (Table 1), generally uses the corresponding magnesocenes and either $MnBr_2$ or $MnI_2(thf)_2$ in tetrahydrofuran except for Me_5C_5, C_5H_5, MeC_5H_4, $(Me_3Si)C_5H_4$, $(Me_3Si)_3C_5H_2$ and $(Me_3C)_3C_5H_2$. In these examples the transfer reagent is either the corresponding potassium or sodium salts of the substituted cyclopentadiene, since the magnesocene reagent did not react cleanly under a variety of conditions investigated with the forementioned cyclopentadienyl derivatives. The manganocenes are soluble in pentane and they are readily purified by crystallization from that solvent. They all sublime from 50-80 °C depending on the substituent under dynamic diffusion pump vacuum, except $(Me_3Si)C_5H_4$ which is a liquid that distils at 92-93 °C in diffusion pump vacuum, and they all give molecular ions in their EI mass spectra. The melting behavior is rather interesting since the melting points increase in the order $(Me_3E)C_5H_4 < (Me_3E)_2C_5H_3 << (Me_3E)_3C_5H_2$, where E= Si or C. Curiously the melting point of $[(Me_3C)(Me_3Si)C_5H_3]_2Mn$ is close to the arithmetic mean of $[(Me_3C)_2C_5H_3]_2Mn$ and $[(Me_3Si)_2C_5H_3]_2Mn$. The colors of the manganocenes are

yellow in the case of $(Me_3Si)C_5H_4$, $(Me_3Si)_2C_5H_3$, $(Me_3Si)_3C_5H_2$ and $(Me_3C)_3C_5H_2$, while the others are orange or red.

Table 1. Characterization data for substituted maganocenes

compound (Cp')	color	m.p. (°C)	T_{sub} (°C) [a]	Mn-C (ave) (Å)	^{1}H NMR (δ) [c]
C_5H_5	amber	172-173		2.41[d]	
MeC_5H_4	amber	62-64			
C_5Me_5	orange	292	90-95	2.11[e]	
$Me_3CC_5H_4$	red	59-60	40-50	2.14[f]	13 (3100)
$Me_3SiC_5H_4$	yellow	< 25	92-93[b]	2.38[g]	13 (524)
1,3-$(Me_3C)_2C_5H_3$	red	145-146	55-60	2.13[f]	15 (2700)
1,3-$(Me_3Si)_2C_5H_3$	ivory	90-91	50-55	2.37[f]	12 (980)
1,2,4-$(Me_3C)_3C_5H_2$	light yellow	308-309	90-95	2.43[f]	15 (2810)
1,2,4-$(Me_3Si)_3C_5H_2$	ivory	286-288	70-80	2.40[f]	10 (1050), 7 (750)
1,3-$(Me_3C)(Me_3Si)C_5H_3$	orange	106-107	50-60		20 (2500) 12 (1750)

[a] sublimation temperature in diffusion pump vacuum; [b] distillation temperature in diffusion pump vacuum at 92-93 °C; [c] Recorded in benzene-d_6 at 20 °C. Chemical shifts of the Me_3E (E= Si or C) resonances in ppm. Line width at half-peak height (Hz) is given in parentheses. Methine resonances are not observed in tetra- and hexasubstituted manganocenes. [d] Averaged Mn-C distance of the η^5-coordinated Cp-ring. Ref. 18. [e] Ref. 16. [f] This work. [g] Ref. 19.

Solid State Crystal Structures. The crystal structures of $[(Me_3Si)_2C_5H_3]_2Mn$, $[(Me_3Si)_3C_5H_2]_2Mn$, $[(Me_3C)C_5H_4]_2Mn$, $[(Me_3C)_2C_5H_3]_2Mn$ and $[(Me_3C)_3C_5H_2]_2Mn$ are determined at low temperature (see Table 2 for details), while that of $[(Me_3Si)C_5H_4]_2Mn$ was reported some years ago.[19] Thus, the solid state structures of the manganocenes described in this paper are known, except for the mixed-ring metallocene $[(Me_3C)(Me_3Si)C_5H_3]_2Mn$; several attempts to grow suitable crystals for an X-ray diffraction study either by slow sublimation or crystallization failed. The ORTEP diagrams are given in

Figures 1-5 and the bond distances and angles are given in the Figure captions (see Supporting Information for details).

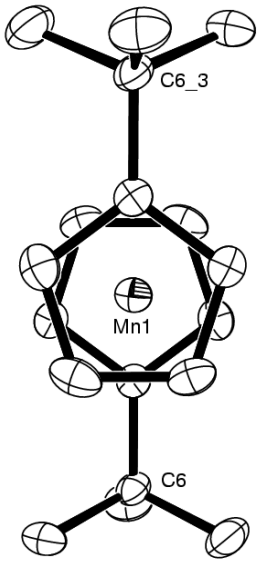

Figure 1. ORTEP diagram of $[(Me_3C)C_5H_4]_2Mn$ (50% probability ellipsoids). Selected distances (Å) and angles (deg): Mn-C (range) 2.117(2)-2.187(2), Mn-$Cp_{centroid}$ 1.77, cyclopentadienyl rings are related by inversion, $Cp_{centroid}$-Mn-$Cp_{controid}$ = 180. Average displacement of quarternary carbon from ring plane is 0.08 Å.

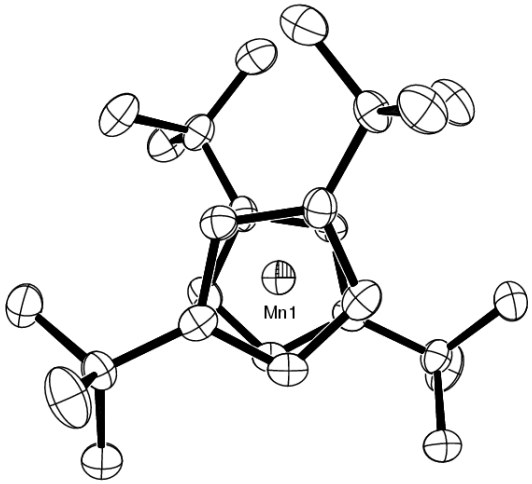

Figure 2. ORTEP diagram of $[1,3\text{-}(Me_3C)_2C_5H_3]_2Mn$ (50% probability ellipsoids). Only one of the unique molecules is shown. Selected distances (Å) and angles (deg): Mn-C (range) 2.072(5)-2.183(5),

Mn-$Cp_{centroid}$ 1.75, cyclopentadienyl rings are related by a C_2 axis, $Cp_{centroid}$-Mn-$Cp_{controid}$ = 175. Average displacement of quarternary carbon from ring plane is 0.16 Å.

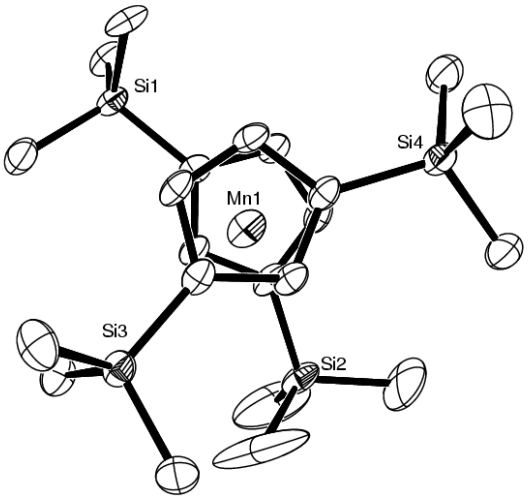

Figure 3. ORTEP diagram of $[1,3\text{-}(Me_3Si)_2C_5H_3]_2Mn$ (50% probability ellipsoids). Selected distances (Å) and angles (deg): Mn-C (range) 2.322(4)-2.408(4), Mn-$Cp_{centroid}$ 2.04, $Cp_{centroid}$-Mn-$Cp_{controid}$ = 166. Average displacement of quarternary carbon from ring plane is 0.06 Å.

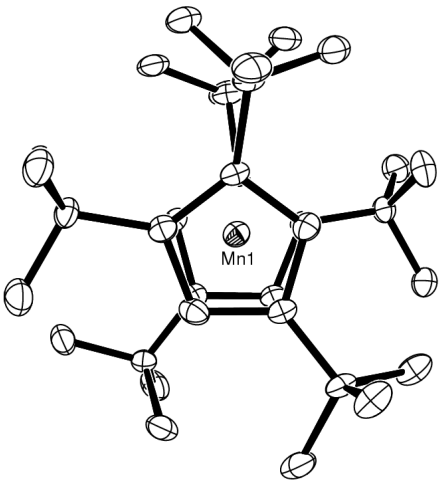

Figure 4. ORTEP diagram of $[1,2,4\text{-}(Me_3C)_3C_5H_2]_2Mn$ (50% probability ellipsoids). Only one of the unique molecules is shown. Selected distances (Å) and angles (deg): Mn-C (range) 2.359(3)-2.487(3),

Mn-$Cp_{centroid}$ 2.11, $Cp_{centroid}$-Mn-$Cp_{controid}$ = 169. Average displacement of quarternary carbon from ring plane is 0.21 Å.

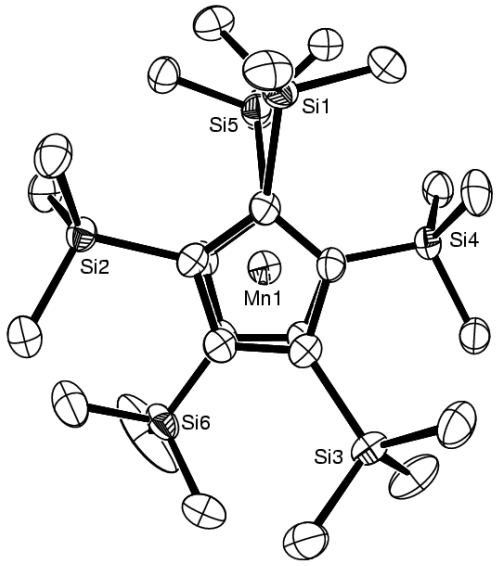

Figure 5. ORTEP diagram of $[1,2,4\text{-}(Me_3Si)_3C_5H_2]_2Mn$ (50% probability ellipsoids). Only one of the unique molecules is shown. Selected distances (Å) and angles (deg): Mn-C (range) 2.350(4)-2.470(4), Mn-$Cp_{centroid}$ 2.07, $Cp_{centroid}$-Mn-$Cp_{controid}$ = 165. Average displacement of quarternary carbon from ring plane is 0.27 Å.

$[(Me_3C)C_5H_4]_2Mn$ has C_{2h} symmetry, the rings are staggered, and the CMe_3 groups point away from each other to reduce intramolecular interactions. The compound is isostructural and isomorphous to its magnesium analogue,[20] whose ionic radius is between that of high-spin and low-spin Mn^{2+}.[21] A similar geometry was reported by Köhler for the $SiMe_3$ analogue.[19] $[(Me_3C)_2C_5H_3]_2Mn$ and $[(Me_3Si)_2C_5H_3]_2Mn$ have idealized C_2 symmetry and the Cp rings are essentially eclipsed and coplanar. In $[(Me_3C)_3C_5H_2]_2Mn$ and $[(Me_3Si)_3C_5H_2]_2Mn$ the Cp rings are essentially eclipsed, the rings are coplanar, and the molecule has idealized C_2 symmetry. A notable feature is that the CMe_3 and $SiMe_3$ groups deviate from the plane defined by five ring carbons by 0.21 and 0.27 Å, respectively.

Although the manganocenes with the same number of Me_3C and Me_3Si groups attached to the C_5 ring have the same idealized symmetry and orientation of the ring substituents, the Mn-C and Mn-Cp(cent) distances differ greatly (Table 1) between these manganocenes. Thus, the Mn-C distances in $(Me_3C)C_5H_4$ and $(Me_3C)_2C_5H_3$ are, on average, 0.24 Å shorter than those in $(Me_3Si)C_5H_4$ and $(Me_3Si)_2C_5H_3$ manganocenes In marked contrast, the averaged Mn-C distances in $(Me_3C)_3C_5H_2$ of 2.43(4) Å are the same as those in $(Me_3Si)_3C_5H_2$ of 2.40(3) Å within 3σ. The differences in the bond distances show that these manganocenes have different spin states, with the shorter distances associated with the low-spin isomer. These distances compare well to those obtained for the high-spin isomer in $(MeC_5H_4)_2Mn$ of 2.433(8) Å and the low-spin isomer of 2.144(12) Å in the gas electron diffraction study. The value of the Mn-C distance in $(Me_5C_5)_2Mn$ of 2.111(3) Å clearly indicates it is low-spin, which is supported by variable temperature magnetic susceptibility data (see below). Thus, Mn-C(ave) distances and the color (yellow to ivory or red) imply high-spin and low-spin, respectively (at the temperature of the observation).

Table 2. Selected Crystal Data and Data Collection Parameters of $[(Me_3C)C_5H_4]_2Mn$, $[1,3\text{-}(Me_3C)_2C_5H_3]_2Mn$, $[1,3\text{-}(Me_3Si)_2C_5H_3]_2Mn$, $[1,2,4\text{-}(Me_3C)_3C_5H_2]_2Mn$ and $[1,2,4\text{-}(Me_3Si)_3C_5H_2]_2Mn$.

Compound	$[(Me_3C)C_5H_4]_2Mn$	$[1,3\text{-}(Me_3C)_2C_5H_3]_2Mn$	$[1,3\text{-}(Me_3Si)_2C_5H_3]_2Mn$	$[1,2,4\text{-}(Me_3C)_3C_5H_2]_2Mn$	$[1,2,4\text{-}(Me_3Si)_3C_5H_2]_2Mn$
Formula	$C_{18}H_{26}Mn$	$C_{26}H_{42}Mn$	$C_{22}H_{42}MnSi_4$	$C_{34}H_{58}Mn$	$C_{28}H_{56}MnSi_6$
FW	297.33	409.54	473.86	521.74	618.22
space group	$P2_1/c$	Pccn	$P2_1/c$	$P2_1/n$	$P2_1/a$
a (Å)	6.101(1)	11.693(1)	10.727(1)	19.326(1)	18.5652(18)
b (Å)	11.141(2)	12.317(1)	12.971(1)	17.640(1)	22.341(2)
c (Å)	11.559(2)	32.877(1)	20.481(1)	20.377(1)	19.5687(19)
β (°)	94.922(2)	90	97.316(1)	112.483(3)	108.735(2)
V ($Å^3$)	782.79(19)	4734.94(15)	2826.49(9)	6418.9(2)	7686.5(13)
Z	2	8	4	8	8
d_{calc} (g/cm^3)	1.261	1.149	1.114	1.080	1.068
μ(Mo-Kα)$_{calc}$	0.83	0.56	0.64	0.42	0.55
Size (mm)	0.30 x 0.21 x 0.20	0.22 x 0.18 x 0.12	0.25 x 0.20 x 0.05	0.28 x 0.23 x 0.12	0.36 x 0.30 x 0.24
temperature (K)	151(2)	138(2)	137(2)	175(2)	131(2)
scan type, θ_{max}	ω, 24.67 °	ω, 23.25°	ω, 25.57°	ω, 24.79°	ω, 24.74°
Reflections integrated	3336	17641	12447	27459	33864
unique reflections, R_{int}	1277, 0.0376	3401, 0.1165	4769, 0.0716	10450, 0.0705	12656, 0.0642

good reflections	1068, $F_o^2>2\sigma(F_o^2)$	2382, $F_o^2>2\sigma(F_o^2)$	3360, $F_o^2>2\sigma(F_o^2)$	6595, $F_o^2>2\sigma(F_o^2)$	8443, $F_o^2>2\sigma(F_o^2)$
Variables	91	257	256	667	694
transmission range	0.937 – 0.680	0.992 – 0.774	0.990 – 0.859	0.950 – 0.889	0.880 – 0.837
R_1[a]	0.0366	0.0687	0.0722	0.0491	0.0532
wR_2[b]	0.0959	0.1287	0.1900	0.1068	0.1275
R_{all}	0.0467	0.1068	0.0956	0.0978	0.0934
GOF (on F^2)	1.052	1.177	1.043	0.981	1.007
max/min peaks in final difference map	0.299/–0.517 $e^-/Å^3$	0.263/–0.477 $e^-/Å^3$	1.544/–0.530 $e^-/Å^3$	0.390/–0.612 $e^-/Å^3$	0.624/–0.623 $e^-/Å^3$

[a] $R_1 = \Sigma||Fo| - |Fc|| / \Sigma|Fo|$. [b] $wR_2 = [(\Sigma w (|Fo|^2 - |Fc|^2)^2 / \Sigma w |Fo|^4)]^{1/2}$

Solid State Magnetic Susceptibility Studies. The spin state deductions derived from the Mn-C distances are supported by the variable temperature magnetic susceptibility studies on these manganocenes over a temperature range from 5 to 300 K. A high-spin manganocene has a $^6A_{1g}$ ground state (in D_{5d} symmetry) and will have an electronic configuration $e_{2g}^2a_{1g}^1e_{1g}^2$ and the expected spin-only value of μ_{eff} is 5.92 μ_B.[22] A low-spin manganocene has a $^2E_{2g}$ ground state with electronic configuration $e_{2g}^3a_{1g}^2$ and the expected effective magnetic moment is about 2.2 μ_B, since there will be an orbital contribution to this moment.[23] The reported effective moment for $[(Me_2CH)_4C_5H]_2Mn$ of 5.72 μ_B is temperature independent from 5 to 350 K, consistent with the high-spin state (S= 5/2) deduced by the Mn-C bond lengths.[24] The effective magnetic moment of $(C_5Me_5)_2Mn$ of 2.17 μ_B from 5 to 100 K[17, 25] is also consistent with low-spin S= ½, as deduced from the Mn-C distances; the magnetic data over a wider temperature range, 5-560 K, is temperature independent, see Supporting Information for details (Figure S6). Thus, the magnetic moment as a function of temperature indicates the spin state for the manganocenes.

The magnetic susceptibility data for the three Me_3Si-substituted manganocenes are plotted as μ_{eff} vs. T, as shown in Figure 6. For $[(Me_3Si)_2C_5H_3]_2Mn$ and $[(Me_3Si)_3C_5H_2]_2Mn$, the magnetic moment, μ_{eff}, is independent of temperature over the temperature range studied, and the value of μ_{eff} is ~ 5.9 μ_B, consistent with a high-spin state throughout the temperature range. The plots of χ^{-1} vs. T, available in Supporting Information, Figure S7, are linear in T, showing that these two manganocenes follow the Curie-Weiss law over the temperature range, $\chi= C/(T-\theta)$, and the θ constants are small, -1.6 K and -1.2 K for $[(Me_3Si)_2C_5H_3]_2Mn$ and $[(Me_3Si)_3C_5H_2]_2Mn$, respectively. The small value of θ implies that they are isolated paramagnets and the negative value of θ indicates weak antiferromagetic spin interactions or zero-field splitting (ZFS). The behavior of $[(Me_3Si)C_5H_4]_2Mn$ is the same as the other two compounds from 300 to 150 K, but below this temperature the value of μ_{eff} experiences a non-linear decrease until 100 K, below which the effective magnetic moment is essentially temperature independent. This suggests that the population of the spin-isomers changes in the temperature regime of 100-150 K, but that the populations are fixed at temperatures below 100 K and above 150 K. The decrease in μ_{eff} below

about 20 K in all samples can be attributed to both weak intermolecular antiferromagnetic coupling and ZFS of the S= 5/2 ground state.[26]

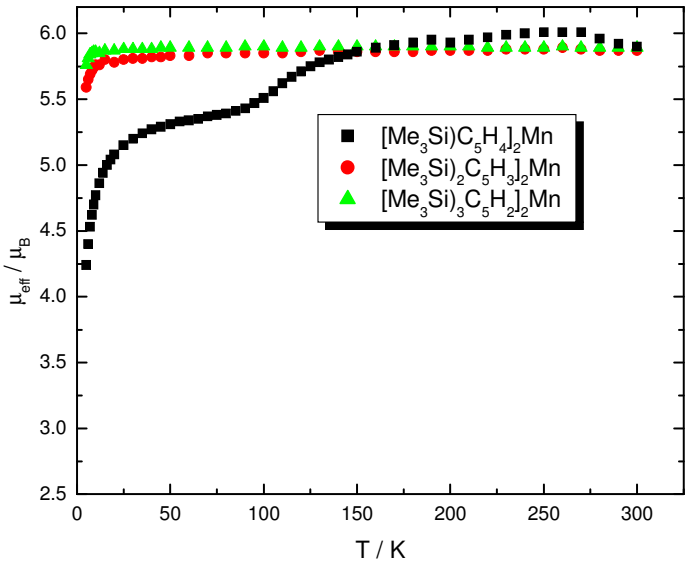

Figure 6. Solid state magnetic moment vs. T plots for $[(Me_3Si)_nC_5H_{5-n}]_2Mn$ (n= 1, 2, 3).

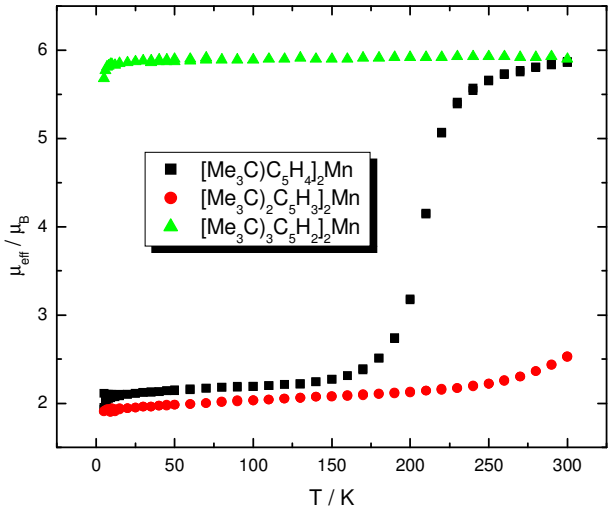

Figure 7. Solid state magnetic moment vs. T plots for $[(Me_3C)_nC_5H_{5-n}]_2Mn$ (n= 1, 2, 3).

The magnetic behavior of the three Me_3C-substituted derivatives is widely different and rather more interesting than $[(Me_3Si)_2C_5H_3]_2Mn$ and $[(Me_3Si)_3C_5H_2]_2Mn$. Figure 7 shows plots of μ_{eff} as a function of temperature to 300 K for the three manganocenes. The behavior of $[(Me_3C)_3C_5H_2]_2Mn$ is like that found for the $[(Me_3Si)_3C_5H_2]_2Mn$ and $[(Me_3Si)_2C_5H_3]_2Mn$ derivatives, viz., μ_{eff} is independent of temperature from 5 to 300 K, and θ= -1.9 K, is similar to that found for $[(Me_3Si)_3C_5H_2]_2Mn$ and $[(Me_3Si)_2C_5H_3]_2Mn$. The magnetic moment and the Mn-C bond distances are consistent with S= 5/2 in this example. The magnetic behavior becomes strongly temperature dependent, however, when the number of Me_3C substituents is decreased by one, giving $[(Me_3C)_2C_5H_3]_2Mn$ whose μ_{eff} vs. T plot is shown in Figure 7. The χ^{-1} vs. T and χT vs. T plots are available in Supporting Information, Figure S8. The value of μ_{eff} in the low temperature range (5-200 K) is essentially independent of temperature and μ_{eff} is ~ 2 μ_B, a value close to that found for $(Me_5C_5)_2Mn$. In addition, since the Mn-C(ave.) bond distances for $[(Me_3C)_2C_5H_3]_2Mn$ and $(Me_5C_5)_2Mn$ are in the same range, these manganocenes have the same spin state, S= ½ . Inspection of Figure 7 shows that μ_{eff} is increasing slightly in the temperature regime of 5 to 250 K at which point the slope appears to increase. When these results were originally obtained, it was not possible to obtain data at T > 300 K (due to the limitations of the sample container). However, using quartz tubes as sample containers (see Experimental Section for details) temperatures up to 700 K are now routinely accessible. The data from 5 to 400 K are shown in Figure 8, where it is clear that μ_{eff} changes quite rapidly over the temperature range 300 to 400 K, so that the value of μ_{eff} approaches that of 5.5 μ_B, i.e. the value expected for a S= 5/2 molecule. Another feature in the μ_{eff} vs. T plot is that cooling of the sample from 400 K does not trace the original heating curve until about 150 K; this manganocene shows a distinct hysteresis between initial heating and cooling curves of 16 K. Subsequent heating and cooling yields moments that follow the initial cooling curve with a smaller hysteresis (ΔT= 2K) and annealing is finally observed as the original cooling curve is obtained after 5-10 cycles. Thus, $[(Me_3C)_2C_5H_3]_2Mn$ appears to be a spin equilibrium molecule with a very wide transition temperature range and a hysteresis implying substantial reorganization of the individual molecules in the crystal as they change their spin state when approaching the melting point of 428-429 K.

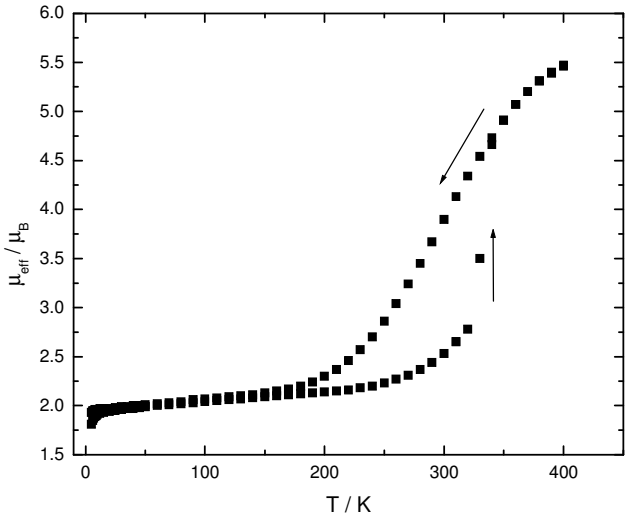

Figure 8. Solid state magnetic moment vs. T plot for $[(Me_3C)_2C_5H_3]_2Mn$. These data were collected on initial heating and cooling.

These results are most consistent with a manganocene whose ground state is $^2E_{2g}$ and the populations of the $^6A_{1g}$ state gradually increasing up to 330 K. At this point $[(Me_3C)_2C_5H_3]_2Mn$ presumably undergoes a crystallographic phase transition with significant structural rearrangements. The phase transition is accompanied by a change in the electronic ground state to an essentially high-spin configuration, where the mole fraction of the high-spin state is $x_{HS.}$= 0.89, as indicated by a moment that approaches the spin-only value for manganese(II) at 400 K. Upon cooling, the populations of the low-spin isomer increases until about 200 K when the population of the high-spin isomer is small. The hysteresis behavior is presumably due to the rate at which the spin isomers change population which in turn is associated with the orientation of the individual molecules in the crystalline lattice, *i.e.*, their space group symmetry. The initial heating and cooling cycle has a relatively large transition temperature associated with it, but progressively smaller as the heating and cooling curves are cycled, presumably due to what is referred to as a decrease in lattice elasticity.[27, 28] The idea that the high- and low-spin isomers crystallize in different space groups is based upon a comparison between the crystal structures of $[(Me_3C)_2C_5H_3]_2Mn$ and $[(Me_3Si)_2C_5H_3]_2Mn$, which are not isomorphous; $[(Me_3C)_2C_5H_3]_2Mn$

crystallizes in the orthorhombic space group, Pccn, and the molecule contains a crystallographic imposed C_2-axis whereas $[(Me_3Si)_2C_5H_3]_2Mn$ crystallizes in the monoclinic space group, $P2_1/c$. Although no crystal structure data are available on the high-spin isomer of $[(Me_3C)_2C_5H_3]_2Mn$, it can be assumed, that this isomer also adopts the more open but less ordered $P2_1/c$ structure. The packing diagrams for $[(Me_3C)_2C_5H_3]_2Mn$ and $[(Me_3Si)_2C_5H_3]_2Mn$ are provided as Supporting Information, Figures S9 and S10. This hypothesis is supported by the close structural relation among $[(Me_3Si)_2C_5H_3]_2Mn$, $[(Me_3Si)_3C_5H_2]_2Mn$ and $[(Me_3C)_3C_5H_2]_2Mn$, which are isomorphous, isostructural and high-spin manganocenes. Phase transitions that convert low-spin Pccn structures into high-spin $P2_1/c$ structures are not without precedent and have been observed in coordination compounds.[29] Furthermore the interconversion of the low-temperature orthorhombic Cmca to the room temperature monoclinic C2/c space group has been observed for $(C_5Me_5)_2Mn$,[30] although no spin-state change occurs. In the next section, we show that variable temperature extended X-ray absorption fine structure (EXAFS) measurements are used to quantify the connection between magnetic moments and bond lengths, which support the qualitative inferences mentioned above.

The magnetic behavior of $[(Me_3C)C_5H_4]_2Mn$ is related to that of $[(Me_3C)_2C_5H_3]_2Mn$ except that the transition temperature is lower, about 200 K, and this manganocene is essentially a S= 5/2 molecule at its melting point (332-333 K), where the color changes from red to yellow-orange on melting. Ammeter has shown by UV/VIS spectroscopy that $[(Me_3C)C_5H_4]_2Mn$ is a spin-equilibrium molecule in solution.[13]

It is clear that the 1,3-$R_2C_5H_3$ ligands induce vastly different magnetic properties on the resulting manganocene depending upon whether R_2 is two Me_3C or two Me_3Si. It is then of interest to prepare a mixed manganocene and examine its magnetic behavior. The isomer $[1\text{-}(Me_3C)\text{-}3\text{-}(Me_3Si)C_5H_3]_2Mn$ was prepared, which exists as a mixture of diastereomers of idealized C_s (*meso*) or C_2 (*dl, rac*) symmetry depending on the face to which the metal is bound (Scheme 1). The two optical active species (C_2) are undistinguishable energetically and magnetically, but the *meso*-isomer has a different free energy and presumably a slightly different spin crossover (SCO) profile.

Scheme 1.

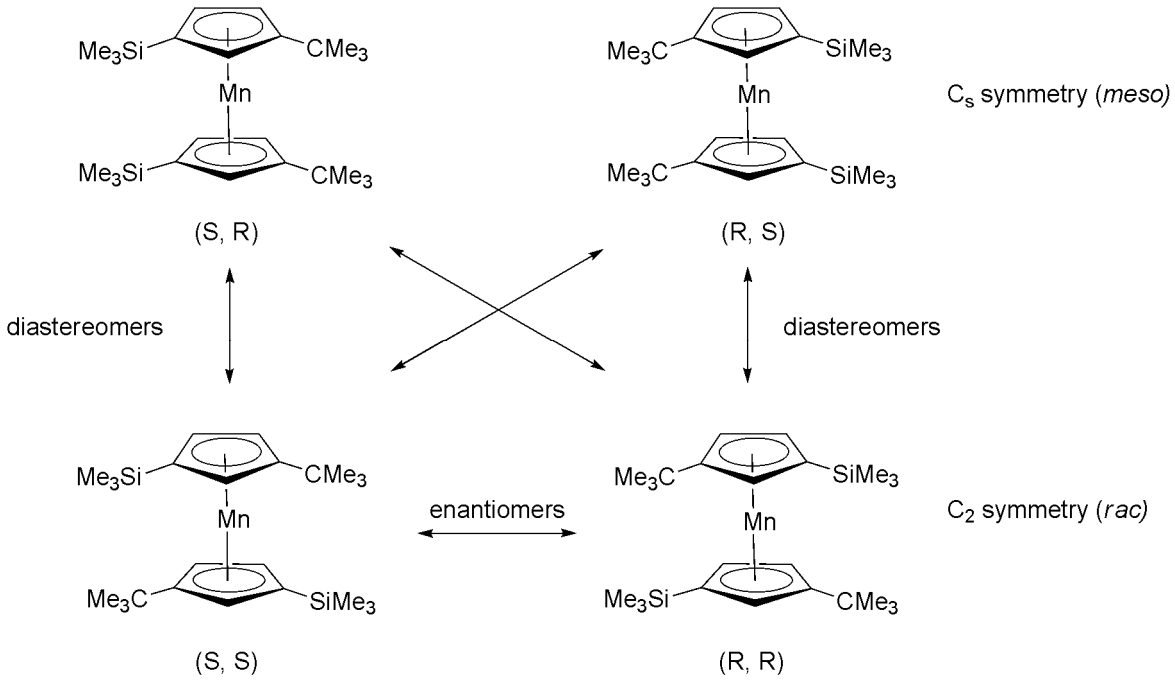

The plot of μ_{eff} vs. T is shown in Figure 9 along with that of Me_3Si with which it is qualitatively similar. At high temperatures, μ_{eff} approaches the value expected for the high-spin isomer. The value of μ_{eff} gradually decreases on cooling to 100 K then the value of μ_{eff} (4.21 μ_B) is essentially independent of temperature to 5 K.

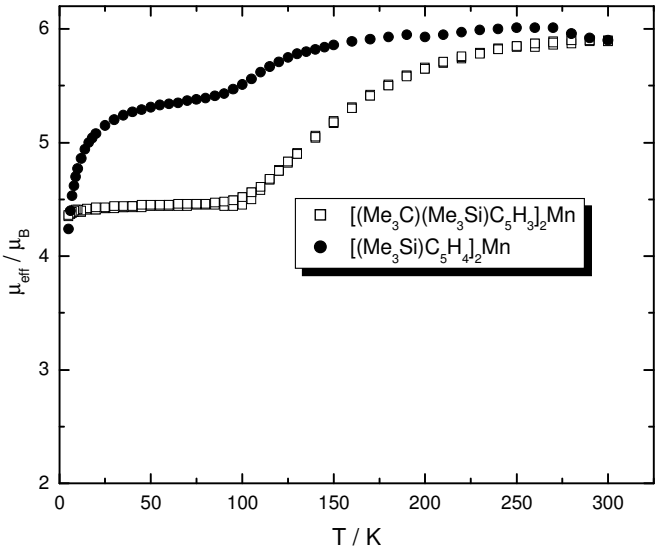

Figure 9. Solid state magnetic moment vs. T plots for $[(Me_3C)(Me_3Si)C_5H_3]_2Mn$ and $[(Me_3Si)C_5H_4]_2Mn$.

The temperature independent region below 100 K depends upon the rate of cooling, as shown in Figures 10 and 11. When the sample is cooled rapidly (10 K/min) from 300 to 5 K (with or without field) and then warmed slowly, the moment is about 4.6 μ_B up to about 90 K, where it subsequently decreases to a minimum value at 105-110 K (μ_B ~ 4.5 μ_B). The moment then smoothly increases to a maximum value of 5.9 μ_B at 300 K. However, if the sample is cooled slowly (1 K/min) from 300 K to 5 K, the magnetic moment agrees well with the rapid-cooled data until about 105 K, where it decreases smoothly to μ_B ~ 4.4 μ_B at 90 K, below which point it is independent of temperature. Although the last stages of the relaxation overlap with the thermal spin-crossover, it is possible to determine a thermal spin-crossover temperature, $T_{1/2}^{thermal}$, of 105 K as defined by Létard and co-workers[31](Figure 11, insert).

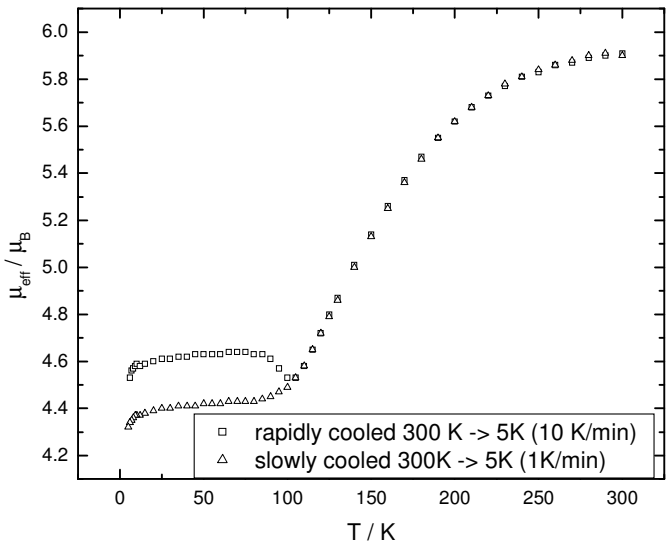

Figure 10. Solid state magnetic moment vs. T plot for $[1,3\text{-}(Me_3C)(Me_3Si)C_5H_3]_2Mn$.

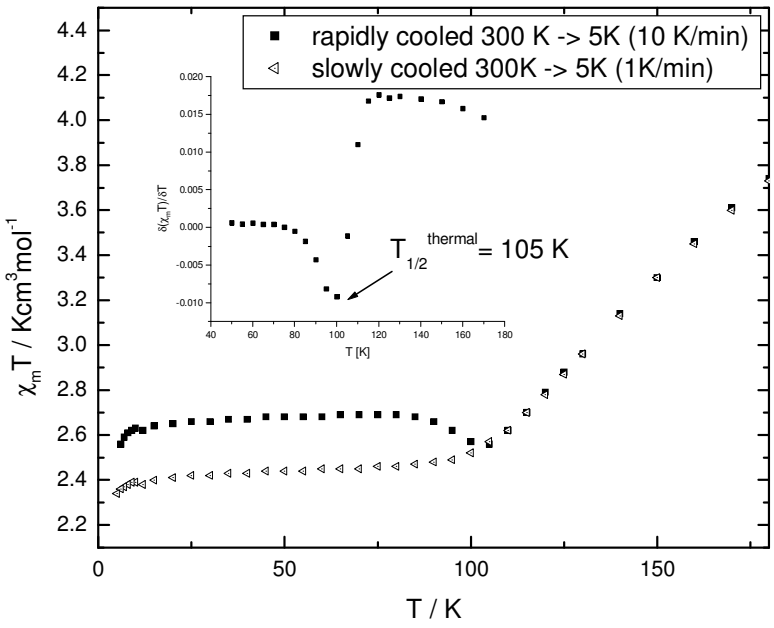

Figure 11. $\chi_m T$ vs. T plot for $[1,3\text{-}(Me_3C)(Me_3Si)C_5H_3]_2Mn$. The insert shows the derivative of the curve after rapid cooling (10 K/min).

It is, in fact, not unusual for magnetic susceptibility to be sensitive to the history of sample. From coordination compounds it is known that a certain quantity of the high-spin population can get trapped

on rapid cooling, because the lattice does not have enough time to relax, a phenomenon known as "spin trapping".[32-39]

Up to 6% of the high-spin population in [1,3-(Me_3C)(Me_3Si)C_5H_3]$_2$Mn can be trapped on cooling 10 K/min and the mole fractions $x_{HS,\ trapped}(5K)= 0.54$ vs. $x_{HS,\ untrapped}(5K)= 0.48$ can be estimated from Figure 11. Relaxation curves in the temperature regime 80-102 K follow first-order kinetics, as expected from isolated metastable species and are provided in Supporting Information (Figure S11). Fitting the experimental curves to an expotential decay law gives satisfactory results for the rate constants *k* for the HS → LS conversion which are gathered in Tabel 3. The ln *k* vs. 1/T plot (Figure S12 in Supporting Information), indicates that the HS → LS relaxation in that temperature regime behaves as a thermally activated process. The linear fit corresponding to a simple Arrhenius law (eq. 1), is excellent (R^2 = 0.996), with A= 20±1 s^{-1}, E_a= 2.13±0.02 kcal mol^{-1} and $\Delta S^{\ddagger}$= - 50.4 cal mol^{-1} K^{-1} (see Supporting Information, Figure S12 for details). The value of 2.13 kcal mol^{-1} for the activation energy (E_a) is of the same order as found for [Fe(1-methyl-tetrazole)$_6$](BF_4), which also exhibits thermal spin trapping.[40]

$$k = A \exp\left(-\frac{E_a}{k_B T}\right) \qquad \text{(eq. 1)}$$

Table 3. High-spin (HS) → low-spin (LS) relaxation rates for [1,3-(Me_3C)(Me_3Si)C_5H_3]$_2$Mn after thermal spin trapping, deduced from a single expotential law.

T [K]	τ [s] x 10^3	k [s^{-1}] x 10^{-5}
80	30.03 ± 0.72	3.33 ± 0.08
85	15.18 ± 0.22	6.59 ± 0.09
90	7.82 ± 0.10	12.79 ± 0.17
95	4.07 ± 0.07	24.60 ± 0.42
100	1.93 ± 0.07	51.91 ± 1.77
102	1.78 ± 0.04	56.30 ± 1.17

EXAFS Study. The EXAFS technique can directly measure the local radial pair-distance distribution function around Mn atoms in these materials, thereby providing a structural parameter, such as distances, to compare with magnetic susceptibility data associated with the Mn spin state. The EXAFS technique has been widely successful in determining the local structure in Fe-based SCO species, for example, see Ref. 41-47. Unlike the studies of Fe compounds, special containment procedures are necessary that present a challenge for obtaining useful EXAFS data on the extremely air-sensitive manganocene compounds, see Experimental Section for details.

In this study, the structural rearrangements in the SCO-hysteresis sample $[1,3\text{-}(Me_3C)_2C_5H_3]_2Mn$ are investigated; data at two temperatures are shown in the Supporting Information, Figure S13. The data range is limited by a monochromator glitch at about 12.5 $Å^{-1}$ that affects data at some temperatures more than others; the samples were very difficult to align because they were strongly tapered. Therefore, the data are fitted to 10 $Å^{-1}$ when direct comparisons of temperature-dependent results are required. The limited data range does not affect the results, as shown below.

The low-temperature *r*-space data show one dominant peak at 1.7 Å, followed by a smaller peak at 2.8 Å (Figure 12). The first peak is due primarily to 10 Mn-C paths (between 2.07-2.18 Å according to diffraction), although there is a small contribution by 6 Mn-H paths (~2.8 Å). Somewhat surprisingly, it is necessary to include these Mn-H paths to allow for a reasonable S_0^2 value (we use S_0^2=0.72 from $CaMnO_3$).[48] The peak at 2.8 Å is due to 4 Mn-C's. The temperature dependence of the Fourier transforms (FTs) is very clear in the raw data, with a sharp drop in amplitude near 330 K.

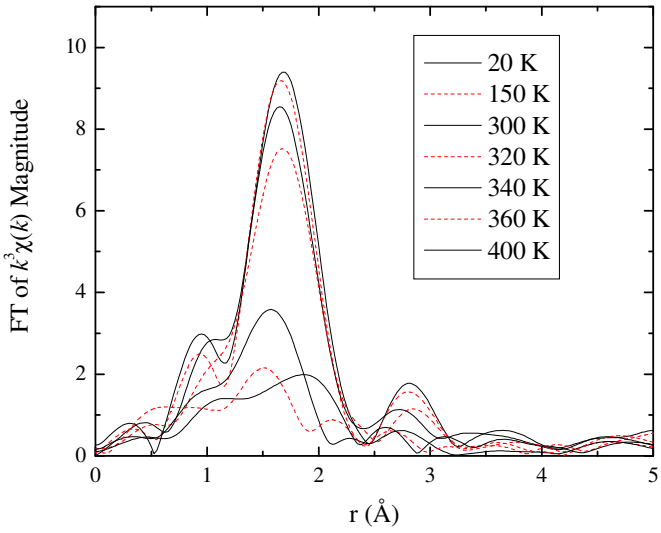

Figure 12. Magnitude of the Fourier transform (FT) of $k^3\chi(k)$. Transform is from 2.5-10 $Å^{-1}$, and Gaussian narrowed by 0.3 $Å^{-1}$.

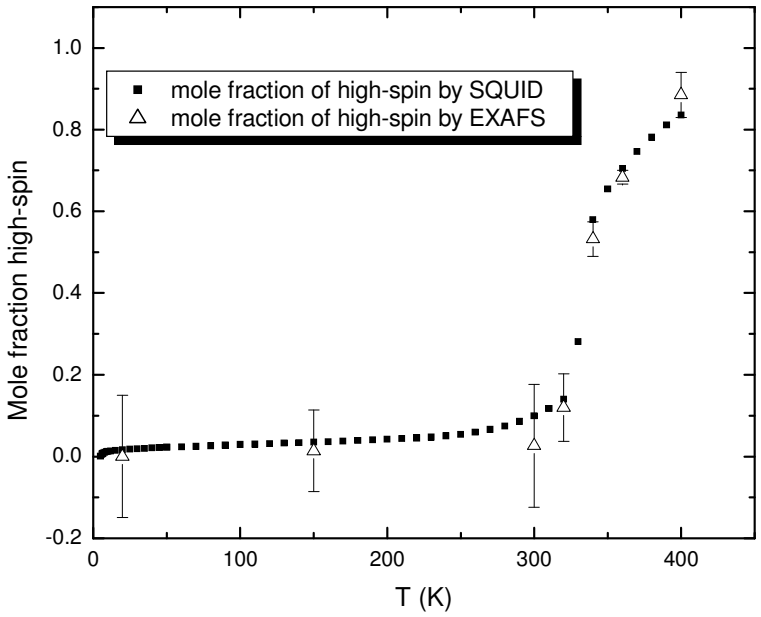

Figure 13. Mole fraction of high-spin isomer vs. T plot, obtained from the relative amplitudes of the two near-neighbor Mn-C shells by EXAFS and magnetic susceptibility studies.

A comparison of the high-spin mole fractions, obtained from the relative amplitudes of the two near-neighbor Mn-C shells and from the solid state magnetism, is excellent, Figure 13.[49] Whereas the EXAFS study provides insight at the molecular level, the magnetic susceptibility reflects a bulk property, yet both methods confirm that a phase transition actually takes place and that it is the origin of the observed hysteresis behavior. After the transformation into the more open, probably "disordered" $P2_1/c$ structure occurs, it is impossible to adopt the original structure on cooling, therefore the spin transition is no longer subject to constraints imposed by the higher symmetry structure and can proceed smoothly over a broader temperature regime. The substituted manganonocene, $[(Me_2CH)_3Me_2C_5)_2Mn$, also exhibits an abrupt spin transition with a hysteresis at 167 K, but no further details are reported, and the molecular origin remains unknown.[50]

EPR Studies. The EPR spectra of manganocenes have been extensively studied, since the low-spin isomers have a $^2E_{2g}$ ground state, which means they are Jahn-Teller molecules. The spectra are usually only observed at very low temperatures, since the spin-lattice relaxation times are long. For the high-spin metallocenes, the zero-field splitting parameter, D, is large (relative to the applied field) and a g-value of about 6 is obtained for MnF_2, MnH_2, MnO,[25, 51-53] and Cp_2Mn in Cp_2Mg[12]. For the low-spin molecules, $g_\parallel$ and $g_\perp$ are observed at values of about 2 (Cp_2Mn in Cp_2Fe, $(C_5Me_5)_2Mn$ in methylcyclohexane glass and doped into $(C_5Me_5)_2Fe$). In this study, the EPR spectra of a representative number of manganocenes are studied as frozen solutions at 4 K in a methylcyclohexane glass (see Supporting Information for details, Figures S14-S16), The manganocene, $[(Me_3Si)_2C_5H_3]_2Mn$, is high-spin to 4 K and it shows a featureless EPR spectrum with a g_{eff}-value of 6.0. The low-spin manganocene, $[(Me_3C)_2C_5H_3]_2Mn$, yields a spectrum with $g_\parallel = 2.57$ and $g_\perp = 1.90$. These two manganocenes follow the expected pattern and the μ_{eff}, determined from EPR spectra, are in agreement with those obtained from SQUID measurements. The EPR spectrum of the mixed manganocene, $[(Me_3C)(Me_3Si)C_5H_3]_2Mn$, substantiates the contention that both spin isomers are present at $T < 100$ K, since a feature due to S= 5/2 state is observed at g= 5.95 and features due to the S= ½ state are observed,

$g_{\|}$= 2.88 and $g_{\perp}$= 1.95. The EPR spectrum clearly supports the proposition that this manganocene exists on the two states, S= 5/2 and S= ½, and the quartet state is not present. Furthermore, the g values for the low-spin isomer can be used to calculate the magnetic moment[54] which agrees with the value measured, as shown in Table 4.

Table 4. Magnetic moments as derived from solid state magnetism and EPR measurements.

Compound	μ_{HS} (by SQUID)	μ_{HS} (by EPR)	μ_{LS} (by SQUID)	μ_{LS} (by EPR)
$[1,3\text{-}(Me_3C)_2C_5H_3]_2Mn$	n/a	n/a	1.91 ± 0.01	1.86 ± 0.02
$[1,3\text{-}(Me_3C)(Me_3Si)C_5H_3]_2Mn$	5.89 ± 0.01	5.86 ± 0.02	n/a	1.99 ± 0.02
$[1,3\text{-}(Me_3Si)_2C_5H_3]_2Mn$	5.88 ± 0.01	5.92 ± 0.01	n/a	n/a

Thermodynamics of SCO

Solid State Studies. Solid state magnetism. Deriving thermodynamic data from solid state susceptibility measurements is rather complicated. In most cases the non-interacting-molecules approach is no longer valid, because the interaction between the different spin-carriers in the assembly has to be included, that is, the cooperativity has to be modeled. A variety of models have been put forward to account for these cooperativity effects, most notably the domain model and the regular solution model.[26] An Arrhenius plot, i.e., the ln K vs. T^{-1} function, provides information about the departure from ideal solution behavior; a linear function is characteristic of the absence of cooperative effects, and deviation from linearity increases with the extent of the interaction.

As shown in Figure S17 in the Supporting Information, the Arrhenius plot for $[1,3\text{-}(Me_3C)_2C_5H_3]_2Mn$ deviates from linearity indicating cooperative behavior. As shown in Figure 7, the magnetic moment, μ_{eff}, is more or less constant up to 210 K (1/T= 0.0047), and then increases smoothly to 5.47 B.M. at 400 K (1/T= 0.0025). This suggests that the population of the high-spin state is small up to 210 K. To get a

rough estimate of the thermodynamic constants for the equilibrium, only the temperature regime from 230-400 K is considered, since this is the temperature range in which the low-spin → high-spin actually occurs. This temperature range is shown in Figure 14. The solution model gives the plot shown in Figure 15.[26] These models do not give fits of high accuracy; additional parameters to account for the interaction must be included, which makes the fit more flexible, but less meaningful in developing a molecular model for the intermolecular cooperativity.

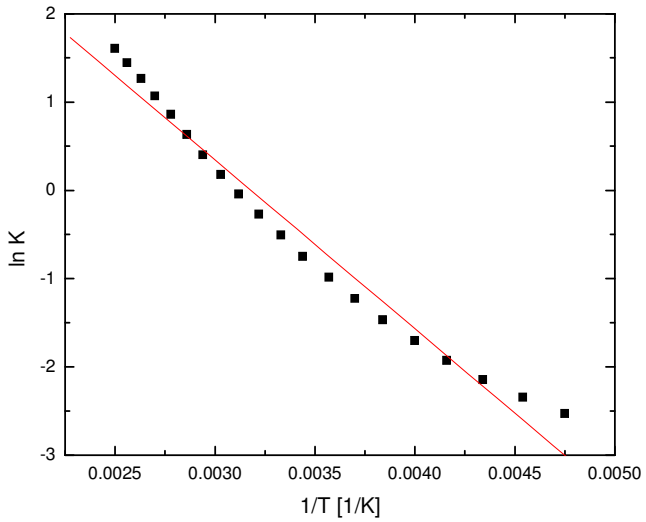

Figure 14. ln K vs T^{-1} plot for high-spin, low-spin equilibrium for $[1,3\text{-}(Me_3C)_2C_5H_3]_2Mn$ determined by solid state magnetic susceptibility after initial phase transformation (230-400 K). The full line represents a fit to a simple linear regression (see text). The obtained fit is moderately good (R^2= 0.973) and gives the values of ΔH^0= 3.8±0.2 kcal/mol and ΔS^0= 12.1±0.5 cal/(mol K).

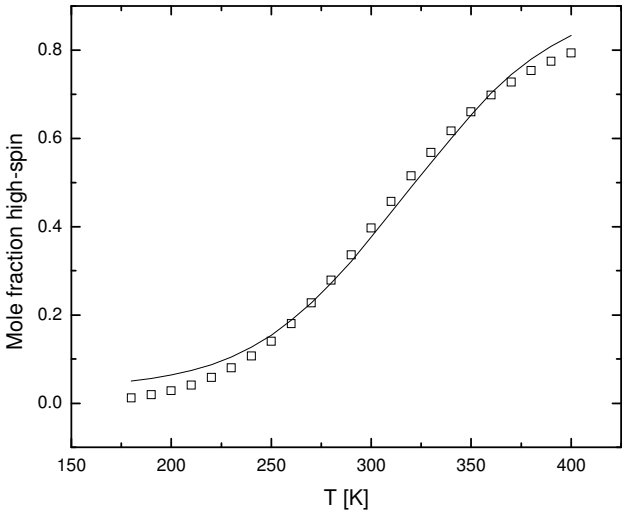

Figure 15. Mole fraction high-spin vs. T plot for high-spin, low-spin equilibrium for [1,3-$(Me_3C)_2C_5H_3]_2Mn$ determined by solid state magnetic susceptibility after initial phase transformation (180-400 K). The full line represents a fit to a regular solution model (see text). ΔH^0= 3.5±0.2 kcal/mol; ΔS^0= 10.6±0.6 cal/(mol K).

The regular solution model was applied to the spin crossover in $[(Me_3C)C_5H_4]_2Mn$, whose thermodynamic properties were evaluated by Ammeter[13] and Köhler[19]. The values for ΔH^0 and ΔS^0 for the solid state are in good agreement to the values obtained by solution studies (Table 5 and Figure S18 in Supporting Information). Fitting the normalized mole fractions vs. T for [1,3-$(Me_3C)(Me_3Si)C_5H_4]_2Mn$ to regular solution models gives a poor fit, although the resulting thermodynamic values are within the expected regime, the mole fraction vs. T plot is available in Supporting Information, Figure S19.

Solution Studies.

UV-vis Studies. Ammeter evaluated the spin-equilibrium in $[(Me_3C)C_5H_4]_2Mn$ by variable temperature UV-vis spectroscopy.[13] This technique also gives thermodynamic data for the SCO in the [1,3-$(Me_3C)_2C_5H_3]_2Mn$ and [1,3-$(Me_3C)(Me_3Si)C_5H_3]_2Mn$ complexes. When the nearly colorless

solution of $[1,3\text{-}(Me_3C)(Me_3Si)C_5H_3]_2Mn$ is cooled in liquid nitrogen, the orange color intensifies significantly, but on warming to room temperature the color fades, implying a reversible equilibrium and the high-spin population is favored at high temperature, whereas the low-spin contribution dominates at low temperature. In free energy terms, the entropy dominates at high temperatures and therefore favors the high-spin species. As the temperature is decreased, the $T\Delta S^0$ term becomes smaller and the enthalpy term dominates the equilibrium.

The fact that high-spin manganocenes are nearly colorless and low-spin species are orange to red allows the equilibrium to be studied using UV-vis spectroscopy. The low-spin complex, $[1,3\text{-}(Me_3C)_2C_5H_3]_2Mn$, exhibits a strong d-d transition ($^2E_{2g} \rightarrow {}^2E_{1u}$)[13] at λ_{max}= 430 nm. For the high-spin isomer, the transition is forbidden.

The variable temperature UV-vis experiment clearly shows an increase in the absorption at 430 nm as the sample is cooled to 170 K (Figure 16). Unfortunately at all temperatures accessible, the low-spin species is in equilibrium with the high-spin species; so the concentration of high-spin and low-spin species at a given temperature is unknown, but the sum is equal to the total concentration. The solid state magnetism indicates that the equilibrium between low- and high-spin $[1,3\text{-}(Me_3C)_2C_5H_3]_2Mn$ shifts to high-spin above 250 K. The absorbance at 269 and 430 nm for high- and low-spin isomers, respectively, are temperature dependent, and the signal at 430 nm shows a significant decrease in absorbance as the temperature is increased whereas the feature at 230 nm increases with temperature.

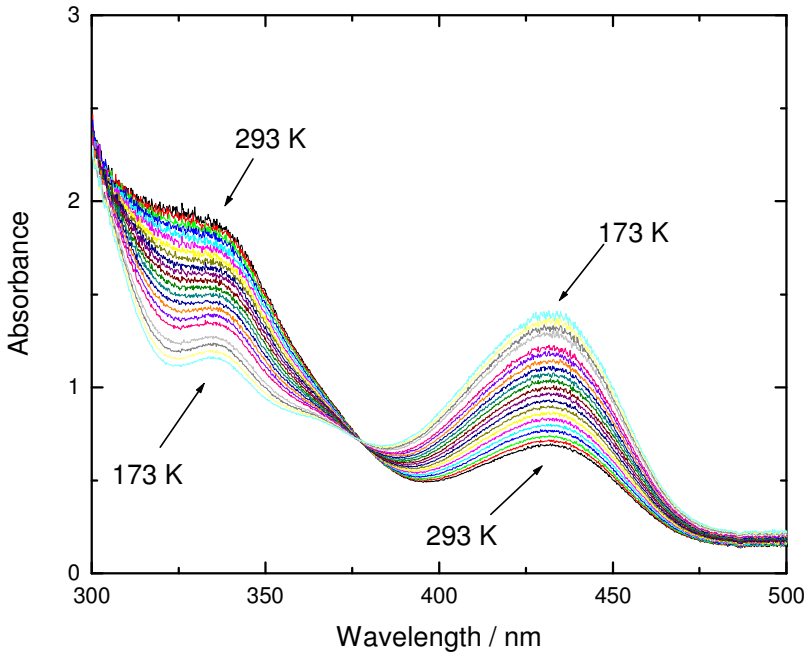

Figure 16. Variable temperature UV-vis spectra for $[1,3\text{-}(Me_3C)_2C_5H_3]_2Mn$.

In order to extract the equilibrium constant, it is assumed that the extinction coefficient of $[1,3\text{-}(Me_3Si)_2C_5H_3]_2Mn$ is, to the first approximation, identical to the extinction coefficient for the high-spin species of $[1,3\text{-}(Me_3C)_2C_5H_3]_2Mn$, since both species exhibit a sharp absorbance at 269 nm. This absorbance with an extinction coefficient is ε = 25 L mol^{-1} cm^{-1} is temperature independent in $[1,3\text{-}(Me_3Si)_2C_5H_3]_2Mn$, consistent with the solid state magnetism, which is high-spin at all temperatures (see Supporting Information for details, Figure S20). This estimate is further corroborated by measuring the extinction of the 330 nm (ε = 2.12 L mol^{-1} cm^{-1}) absorption, which is also temperature invariant in $[1,3\text{-}(Me_3Si)_2C_5H_3]_2Mn$; the values obtained for the concentration of the high-spin form agree in both cases. The thermodynamic data of this spin equilibrium is determined by estimating the value of the extinction coefficient, at the lower temperature limit of the experiment. The absorbance of $[1,3\text{-}(Me_3C)_2C_5H_3]_2Mn$ at 430 nm changes little with temperature and the populations of the isomers are determined from the absorbance data. Furthermore, in solution, the spin conversion is essentially the

property of the individual, isolated molecule and the thermodynamics can be evaluated by assuming non-interacting molecules (eqs. 2 and 3); the lnK vs. T^{-1} plot is shown in Figure 17.

$$K = \frac{x_{h.s.}}{1 - x_{h.s.}} = e^{-(\Delta G^0 / RT)} \qquad \text{(eq. 2)}$$

$$ln\, K = -\frac{\Delta H^0}{RT} + \frac{\Delta S^0}{R} \qquad \text{(eq. 3)}$$

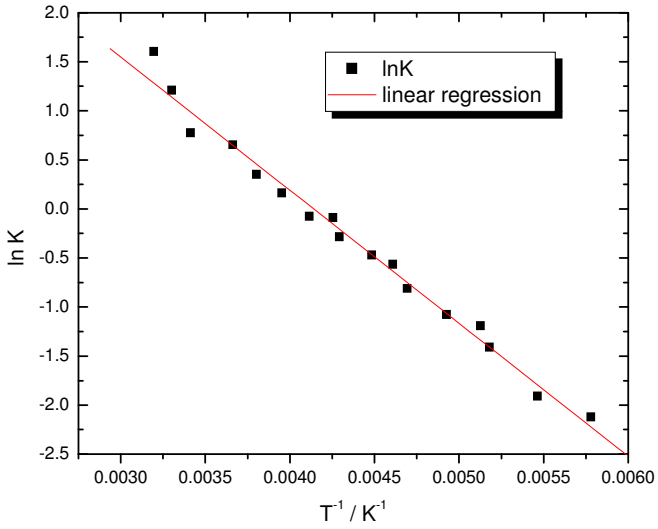

Figure 17. ln K vs T^{-1} plot for high-spin low-spin equilibrium of $[1,3\text{-}(Me_3C)_2C_5H_3]_2Mn$ determined by UV-vis spectroscopy. The thermodynamic values of $\Delta H^0 = 2.7 \pm 0.1$ kcal mol^{-1} and $\Delta S^0 = 11.2 \pm 0.4$ cal mol^{-1} K^{-1} are obtained by a least squares fit ($R^2 = 0.986$).

Evaluating the thermodynamic constants for $[1,3\text{-}(Me_3C)(Me_3Si)C_5H_2]_2Mn$ is more complicated, since the complex exists as a mixture of four different isomers that are divided into 2 pairs of enantiomers of C_2 (*rac*) or C_s (*meso*) symmetry, respectively (see above). The two optical active species (C_2) have the same free energy as do the *meso*-isomers but the *rac*- and *meso*-isomers do not have identical free energies. This complication manifests itself in the fact that although the plot of absorbance at 430 nm vs. T of $[1,3\text{-}(Me_3C)(Me_3Si)C_5H_2]_2Mn$ shows that very little of the low-spin species is present at room

temperature (see Supporting Information, Figure S21), the Arrhenius plot of lnK vs T^{-1} for [1,3-$(Me_3C)(Me_3Si)C_5H_2]_2Mn$ is significantly curved, suggesting that more than two species are involved in the equilibrium in contrast to [1,3-$(Me_3C)_2C_5H_3]_2Mn$ (see Supporting Information, Figure S22). Since it is not possible to determine the population changes of the four isomers, a linear approximation of the curve, to a first approximation, gives enthalpy and entropy changes similar to those obtained previously, Table 5.

Table 5. Thermodynamic Properties of the SCO in Various Manganocenes

Compound	method	K (300 K)	ΔG^0 (300K) (kcal mol^{-1})	ΔH^0 (kcal mol^{-1})	ΔS^0 (cal mol^{-1} K^{-1})	$T_{1/2}$[d] [K]
$[(Me_3C)C_5H_4]_2Mn$	χ (solid)[a]	10.5	-1.4	3.1 ± 0.2	14.9 ± 0.4	211
	χ (solution)[b]	7.5	-1.2	2.0	10.5	194
	UV-vis[b]	2.3	-0.5	3.7	13.9	266
	^1H NMR[c]			2.6-3.2	9.6-12.0	
$[(Me_3C)_2C_5H_3]_2Mn$	χ (solid)[a]	0.7	0.2	3.8 ± 0.2	12.1 ± 0.5	314
		0.7	0.3	3.5 ± 0.2	10.6 ± 0.6	327
	UV-VIS[a]	3.2	-0.7	2.7 ± 0.1	11.2 ± 0.4	241
$[(Me_3C)(Me_3Si)C_5H_3]_2Mn$	χ (solid)[a]	17.3	-1.7	1.7 ± 0.1	11.4 ± 0.5	148
	UV-VIS[a]	47.4	-2.3	3.1 ± 0.1	18.0 ± 0.5	174

[a] This work., [b] Ref. 13, [c] Ref. 19, [d] $T_{1/2} = \Delta H^0/\Delta S^0$ ($\Delta G^0 = 0$)

Model that rationalizes the substituent effects. Manganese(II) has a d^5-electron configuration that gives rise to two possible d-electron configurations in D_{5d} symmetry, *viz.*, $^2E_{2g}$ (e_{2g}^3 a_{1g}^2) or $^6A_{1g}$ (e_{2g}^2 a_{1g}^1 $(e_{1g}^*)^2$) low-spin or high-spin states, respectively. The choice depends upon the energy difference between the $e_{2g}a_{1g}$ and the e_{1g}^* configurations (Δ) and the spin-pairing energy (P), Figure 18.

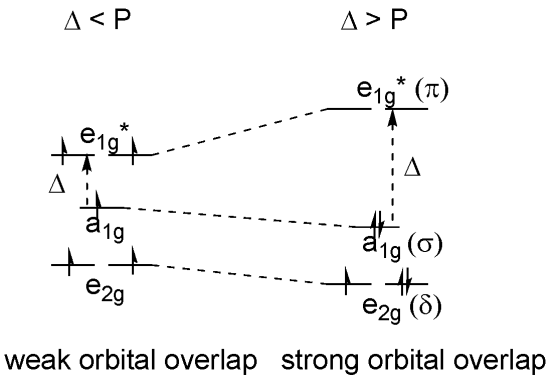

Figure 18. Frontier orbital scheme for d^5-metallocene with idealized D_{5d} symmetry

In general, the results observed for the metallocenes described in this article are that Me_3Si groups favor high-spin manganocenes and Me_3C groups favor either low-spin or spin-equilibrium manganocenes. This electronic effect can be traced to the classification of a Me_3Si group as an electron withdrawing substituent and the Me_3C group as an electron donating substituent deduced from EPR studies on the substituted cyclopentadienyl radicals. Figure 19 shows how these substituents change the relative energy of Ψ_s.[55, 56]

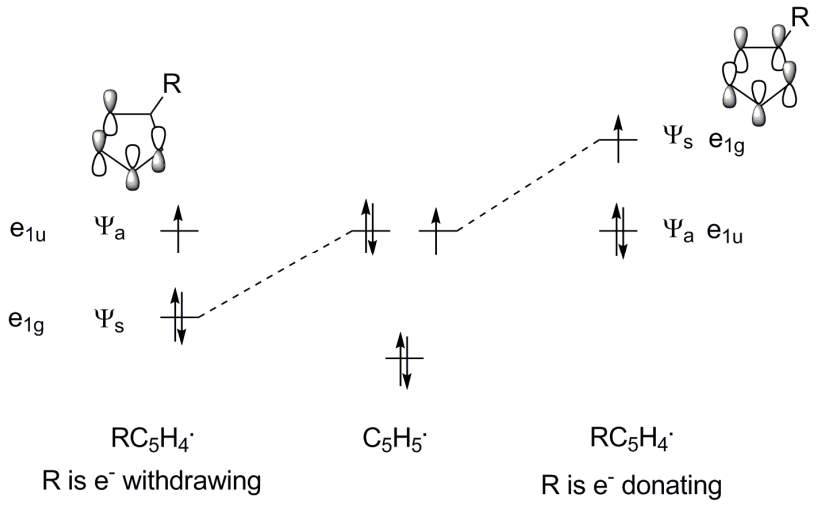

Figure 19. Influence of substitution on the cyclopentadienyl ring on its frontier orbitals.[56]

In a mono-substituted cyclopentadienyl radical a substituent on C(1) does not change the energy of Ψ_a, because it lies on the nodal plane, however, Ψ_s is affected, since C(1) contains electron density. The p_π-electron density at each of the carbon atoms in the cyclopentadienyl ring is determined from the value of the electron-nuclear coupling constant in the radical and is correlated with how the substituents change the relative energy of Ψ_a and Ψ_s. The EPR results show that π-electron withdrawing groups stabilize Ψ_s, whereas π-electron donating groups destabilize Ψ_s. In D_{5d}, Ψ_s has e_{1g} symmetry, which is the same symmetry as the d_{xz} and d_{yz} atomic orbitals used in metallocene bonding. Interaction of the e_{1g} orbitals on the metal and the ligand fragments generates a bonding (e_{1g}) and an antibonding (e_{1g}*) combination. When R is electron donating, the energy of Ψ_s is closer in energy to that of the metal d_{xz} and d_{yz} orbitals and the resulting molecular orbitals will be stabilized (e_{1g}) and destabilized (e_{1g}*) relative to when the substituent is H. The result is that Δ is increased resulting in a low-spin manganocene. Conversely, when R is electron withdrawing, Δ decreases resulting in a high-spin manganocene. This qualitative molecular orbital model is similar to that advanced by Köhler.[19] This model traces the control of spin states to electronic effects, however steric effects do play a role particularly when the number of Me_3C substituents is greater than two; $[1,2,4\text{-}(Me_3C)_3C_5H_2]_2Mn$ is high-spin at all the temperatures examined, a fact that is most reasonably ascribed to steric repulsion between the rings that enforces longer Mn-C bond distances and lowers Δ. Steric effects are also suggested to rationalize the high-spin behavior of $[(Me_2CH)_4C_5H]_2Mn$.[24,50]

Conclusion

The magnetic properties of manganocenes have interested chemists since the first manganocene, $(C_5H_5)_2Mn$, was prepared and studied by Wilkinson[1, 7] and Fischer[3] and their co-workers. Although $(C_5H_5)_2Mn$ is a zig-zag polymer in the solid state, bulky substituents on the cyclopentadienyl rings result in monomers whose magnetic moments depend on their type and number. The two manganocenes described in detail in this article, $[(Me_3C)_xC_5H_{5-x}]_2Mn$, x= 1, 2, are classic textbook examples of spin-equilibrium molecules whose thermodynamic constants are determined in the solid state and in solution

by magnetic susceptibility and UV-vis spectra as function of temperature, respectively. However, these two physical techniques do not provide structural information as the molecules change their spin-states as the single crystal X-ray structures are only done at one temperature. Molecular structural information is, however, provided by EXAFS data as a function of temperature on $[(Me_3C)_2C_5H_3]_2Mn$, since the Mn-C bond distances and therefore the mole fraction of the high-spin isomer (or low-spin isomer) is determined directly. A plot of the mole fraction determined from the EXAFS data coincides with that obtained from the magnetic susceptibility data, as measured by χ, as a function of temperature, Figure 13. This correlation provides a direct measure of the molecular structural changes as the molecules in the solid state ensemble change their spin state. The combination of all of these physical techniques studied in this article provides a detailed molecular level of understanding of $[(Me_3C)_2C_5H_3]_2Mn$ as it isomerizes.

Experimental Section

General Comments. All reactions, product manipulations, and physical studies were carried out as previously described.[57-59] Magnetic measurements were conducted in a 7 T Quantum Design MPMS magnetometer utilizing a superconducting quantum interference device (SQUID). Between 10 and 25 mg of sample were sealed in evacuated quartz tubes held in place with ~5 mg of quartz wool. This method provided a very small and reliable container correction, typically of about -2×10^{-5} emu/mol. The data were also corrected for the overall diamagnetism of the molecule using Pascal constants.[60] For a more detailed description see ref. [58]. GC-MS analysis was performed on a Hewlett-Packard HP 6890 Series GC-System with HP 5973 Mass-Selective Detector. Routine UV-vis spectra were recorded on a Varian Cary 5G spectrometer. The following compounds were prepared as previously described: $(Me_3C)C_5H_5$,[61], $[1,3\text{-}(Me_3Si)_2C_5H_3]_2Mg$,[62] $[1,3\text{-}(Me_3C)_2C_5H_3]_2Mg$,[63, 64] $NaNH_2$,[65] and $(Me_3C)_3C_5H_3$.[66] Dibutylmagnesium was purchased as a heptane solution from Aldrich, and its concentration was determined by titration.

Variable temperature UV-visible Studies. The variable temperature UV-vis spectra were collected using a low temperature apparatus of our own construction. The sample holder for an Ocean Optics ST 2000 fiber optic UV-vis spectrometer was connected to a copper coil arranged so that the coil could be immersed in a liquid N_2 cold bath. During the experiment, dry N_2 was allowed to flow through the copper coils and then through the cell holder. The sample holder was contained in an acrylic box that was purged with dry N_2 to minimize water condensation. A quartz cuvette was fitted with a greaseless stopper that contained an opening through which a thermocouple was inserted and sealed with epoxy. During a typical experiment, the cuvette containing the solvent (methylcyclohexane), with and without solute (for background spectra) was placed into the cell holder inside the acrylic box and the container was purged with dry N_2. The copper coil was placed inside a Dewar flask and cooled with liquid N_2, while the coil was purged with dry N_2. The temperature, which was monitored by the thermocouple in the cuvette, was regulated by the dry N_2 flow rate. A typical experiment consisted of 20-50 data points between the temperature range of 30 to -110 °C over a time period of about 3 h. The collection time for each spectrum was 3-5 ms and the spectra were collected at a given temperature until no change in absorbance was observed.

EXAFS Studies. Preparing the $[1,3\text{-}(Me_3C)_2C_5H_3]_2Mn$ complex for X-ray absorption measurements required mixing about 17 mg of sample (corresponding to a change in absorption at the Mn K edge of about 1.5 absorption lengths) with dried boron nitride in an inert N_2 atmosphere glove box and loading it into a slotted, multiple-sample aluminum holder with lead-wire sealed aluminum windows. This holder guarantees the sample integrity during transportation in a container filled with nitrogen during transport to the Stanford Synchrotron Radiation Laboratory (SSRL) and handling in air (only about one minute) while loading the sample holder into an evacuated LHe-flow cryostat. X-ray absorption data were collected on beam line 11-2 using an unfocused, uncollimated beam with energy resolution (< 0.5 eV) far narrower than the energy width of the edge due to the Mn 1s core-hole lifetime ($E_\tau \approx 1.2$ eV).[67] Data were collected at temperatures between 30 and 400 K using a 60%-tuned Si 220 double crystal monochromator and a harmonic rejection mirror. The EXAFS function was extracted from the raw data

and fit to theoretical backscattering functions calculated by the FEFF8 code[68] with the RSXAP analysis package.[69]

The amplitude of the first peak vs. temperature is shown in the Supporting Information, Figure S23, demonstrating the loss in amplitude above 330 K. Moreover, there is also a shift of weight in the first peak of the FT to higher distances above 330 K, Figure 12. Finally, the data were collected in a second temperature cycle, and they show that the amplitudes at the end temperatures remain as from the first cycle, but the transformation occurs at a lower temperature in the second cycle, since the 300 K data have a much smaller amplitude than before. Fits to the *r*-space data are between 2.5-10 $Å^{-1}$, Gaussian narrowed by 0.3 $Å^{-1}$, and 1.2-3.3 Å. The fits assume the main Mn-C pairs are split into 2 shells: one near 2.1 Å that includes the Jahn-Teller (JT) split nearest neighbors and one near 2.4 Å that occurs in the high-spin state. The pair-distance distribution variance σ^2 of the first peak has little temperature dependence, consistent with a relatively high Einstein temperature Θ_E, but with an offset consistent with the presence of static disorder, as expected from the Jahn-Teller distortion. As the sample passes through the HS/LS transition, it is not possible to obtain an unambiguous σ^2 due to a strong correlation between the relative amplitudes of the two Mn-C scattering shells and their σ^2 fit parameters. Therefore, the σ^2's are arbitrarily set according to the Einstein model with Θ_E= 740 K and σ_{static}^2=0.00340 $Å^2$. The σ^2 parameter for the second peak is allowed to float, and the total number of neighbors in the two peaks is set to 10. This procedure should provide an accurate idea of the fraction of the sample in the high-spin state by comparing the relative scattering amplitude of the two Mn-C near-neighbor shells. The fit quality is reasonably good (see Supporting Information for details, Figure S24 and Figure S25). Fit results, including the bond lengths (Figure S26 in the Supporting Information) are also reasonable. Reported errors are obtained by fitting several data sets at a given temperature, and therefore indicate reproducibility. Systematic errors for these data are expected to be about 0.005 Å in the bond length and 5% in σ and the number of neighbors.[70]

Cyclopentadienes.

$(Me_3Si)C_5H_5$.[71] A 2 L 3-necked flask equipped with a overhead stirrer, jacketed pressure-equalising dropping addition funnel and a reflux condenser was charged with 1100 mL of diethyl ether. Potassium metal (60 g, 1.54 mol) was cut into small pieces and added to the diethyl ether. The flask was cooled in a ice-water bath and freshly cracked cyclopentadiene (100 g, 1.52 mol) was added slowly to the vigorously stirred reaction mixture. H_2 evolved, and the solution turned orange brown as the cyclopentadiene was added over a time period of *ca.* 1.5 h. Stirring was continued for an additional 30 min to ensure complete reaction of the potassium metal. Freshly distilled trimetylsilylchloride (167 g, 1.54 mol) was charged into the dropping funnel and slowly added (over *ca.* 15 min) to the red-brown solution that turned cloudy and pink in color. The slurry was stirred overnight, filtered, residue washed with dry diethyl ether and fractionally distilled to give yields greater than 70-80 %; the entire procedure was carried out under rigorously exclusion of air and moisture. Synthesis according to literature procedure[72] invariably gave a product heavily contaminated with tetrahydrofuran and water.

$(Me_3Si)_2C_5H_4$. $(Me_3Si)_2C_5H_4$ was prepared from $(Me_3Si)C_5H_5$ using a similar procedure as described for $(Me_3Si)C_5H_5$ yielding a colorless liquid in greater than 70 % yield. Bis(trimethylsilyl)cyclopentadiene has been prepared using another route.[73]

$(Me_3C)_2C_5H_4$. Di(1,3-tert-butyl)cyclopentadiene, $[(Me_3C)_2C_5H_4]$, was prepared in a modified version of the synthesis reported by Venier and Casserly[74]: Potassium hydroxide (1 kg, 25 mol) was dissolved in 750 mL of water in a 3-L, 3-necked flask equipped with an overhead stirrer. The potassium hydroxide solution was allowed to cool to room temperature and Adogen 464 (5g), freshly cracked cyclopentadiene (100 mL, 1.21 mol) and tert-butyl bromide, Me_3CBr, (300 mL, 2.65 mol), were added. In contrast to the reported procedure, better yields have been obtained by sequential addition of tert-butyl bromide as follows. The reaction mixture was stirred vigorously for 12 h at 60 °C. An additional 50 mL (0.44 mol) of Me_3CBr was added and the mixture was stirred for another 24 h at 60 °C, followed by addition of another 50 mL of Me_3CBr and further stirring. Progress of the reaction was monitored by gas chromatography (GC) and after 4-5 days, only 5% of $(Me_3C)C_5H_5$, and no C_5H_6 remained in the mixture. The organic layer was separated and washed with 1 M HCl (100 mL). The product was dried

over anhydrous $Mg(SO_4)$ and distilled at 40 °C (10^{-2} torr). The product was analyzed by GC and was typically > 98 % pure $(Me_3C)_2C_5H_4$ (150 g, 0.841 mol, 70 % yield).

(1-Me_3Si)(3-Me_3C)C_5H_4. The magnesocene, $[(Me_3C)C_5H_4]_2Mg$, (74 g, 0.28 mol) was dissolved in tetrahydrofuran (100 mL) and freshly distilled trimethylsilylchloride (71.1 ml, 60.84 g, 0.56 mol) was added dropwise. The reaction was noticeably exothermic and a colorless precipitate formed before the addition was complete. The mixture was heated to reflux for 5 hours to insure complete conversion of the magnesocene. Filtration, removal of the solvent under reduced pressure and distillation of the product at 38-41 °C in oil pump vacuum yielded a colorless liquid (105 g, 0.54 mol, 96 %). Anal. calcd. for $C_{12}H_{22}Si$: C, 74.17; H, 11.41. Found: C, 74.99; H, 11.96. The E.I. mass spectrum showed a parent ion at m/e = 194 amu. 3-tert-butyl(1-trimethylsilyl)cyclopentadiene has been prepared using another route.[75]

2,5,5-(Me_3Si)$_3C_5H_4$. The magnesocene, $[1,3\text{-}(Me_3Si)_2C_5H_3]_2Mg$, (15 g, 33.8 mmol) was dissolved in tetrahydrofuran (100 mL) and freshly distilled trimethylsilylchloride (8.6 ml, 7.34 g, 67.6 mmol) was added dropwise. The mixture was heated to reflux for 12 h. Cooling to room temperature, filtration, removal of the solvent under reduced pressure and distillation of the product at 55-62 °C in oil pump vacuum yielded a pale yellow liquid (16.6 g, 58.7 mmol, 87 %). The product was analyzed by GC-MS and was typically > 98 % pure. The NMR spectroscopic data agree with that reported previously.[76]

Magnesocenes and Sodium Cyclopentadienides.

$[(Me_3C)C_5H_4]_2Mg$. 1,1‘-Di(tert-butyl)magnesocene, $[(Me_3C)C_5H_4]_2Mg$, was synthesized by treating mono(tert-butyl)cyclopentadiene (100 g, 0.82 mol) with a heptane solution of dibutylmagnesium (470 mL, 0.87 M, 0.41 mol). The solution became warm and gas evolution was vigorous. The mixture was stirred at room temperature for 12 h. The solution was filtered and concentrated to a volume of 250 mL and slowly cooled to −80 °C. Colorless crystals were isolated (69 g, 63 %). A second crop of crystals (15 g) was obtained by concentrating the mother liquor and cooling to –20 °C. Overall yield: 84 g (0.315 mol, 77 %). M.p. 93-95 °C. $[(Me_3C)C_5H_4]_2Mg$ sublimes at 75-80 °C in oil pump vacuum. The NMR spectroscopic data agree with that previously reported for this compound.[20]

$[(Me_3Si)C_5H_4]_2Mg$. 1,1'-Bis(trimethylsilyl)magnesocene, $[(Me_3Si)C_5H_4]_2Mg$, was synthesized by treating mono(trimethylsilyl)cyclopentadiene (19.6 g, 0.142 mol) with a heptane solution of dibutylmagnesium (11.4 mL, 0.625 M, 0.071 mol). The mixture was heated at gentle reflux for 3 hours. The solution was cooled to room temperature, filtered and the solvent removed under reduced pressure leaving behind a light yellow oil. In contrast to a previous report,[62] pure $[(Me_3Si)C_5H_4]_2Mg$ was obtained as a colorless, viscous liquid by distillation in diffusion pump vacuum with a bath temperature of 80-100 °C (13.04 g, 0.04 mol, 57 %). ^{1}H NMR (C_6D_6, RT, 400 MHz): δ 6.25-6.20 ppm (m, AA'BB', $H_{2,2'}$ and $H_{3,3'}$, 4H, ring-C*H*), 0.26 ppm (s, 9 H, Si(CH_3)$_3$).

$[(3\text{-}Me_3C)(1\text{-}Me_3Si)C_5H_3]_2Mg$. To 3-tert-butyl(1-trimethylsilyl)cyclopentadiene (110 g, 0.57 mol) was added a solution of dibutylmagnesium in heptane (320 mL, 0.87 M, 0.28 mol). The mixture was heated to reflux and the butane evolution was monitored with an oil bubbler. After 12 h the reaction was complete as determined by isolation of the system from the oil bubbler for ten minutes without generation of pressure. The solution was filtered and slowly cooled to –80 °C. Colorless crystals were obtained (88 g). The mother liquor was concentrated to a volume of 50 mL and cooled to produce a second crop of crystals (6.4 g). Overall yield: 94.4 g, 0.23 mol, 82 %). M.p. 107-108 °C (rev) [Lit.: 99 °C.[Schumann, 2001 #17]] Sublimation: 95-100 °C (oil pump vacuum). IR (Nujol mull; CsI windows; cm^{-1}): 1330w, 1290w, 1250s, 1205w, 1180m, 1170m, 1085m, 1055m, 1025w, 945m, 930m, 835s, 825s, 755s, 725w, 690m, 650w, 635m, 510m, 485m, 450w, 430m, 360w, 340w, 325w, 290w. ^{1}H NMR (C_6D_6, 500 MHz): 0.301 (18H, s), 0.308 (18H, s), 1.30 (18H, s), 1.31 (18H, s), 6.16 (2H, dd, $^4J_{HH}$= 2Hz, $^4J_{HH}$= 2Hz), 6.16 (2H, dd, $^4J_{HH}$= 2 Hz, $^4J_{HH}$= 2Hz), 6.21 (2 H, dd, $^3J_{HH}$= 10 Hz, $^4J_{HH}$= 2 Hz), 6.20 (2 H, dd, $^3J_{HH}$= 10 Hz, $^4J_{HH}$= 2 Hz), 6.28 (2 H, dd, $^3J_{HH}$= 10 Hz, $^4J_{HH}$= 2 Hz), 6.28 (dd, $^3J_{HH}$= 10 Hz, $^4J_{HH}$= 2 Hz). ^{13}C-NMR (C_6D_6, 125.8 MHz): 138.72 (C_5CCH_3), 138.58 (C_5CCH_3), 115.56 (C_5SiCH_3), 115.36 (C_5SiCH_3), 114.74 (2-C_5H), 114.65 (2-C_5H), 110.14 (4-C_5H), 110.11 (4-C_5H), 108.52 (5-C_5H), 108.50 (5-C_5H), 32.54 (CCH$_3$), 32.44 (CCH$_3$), 32.38 (CCH$_3$), 0.521 (SiCH$_3$), 0.517 (SiCH$_3$). The variable temperature ^{1}H-NMR spectrum does not exhibit any line shape changes between 30 °C and 120 °C and therefore the population of the *meso*- and *dl*-isomer does not change. Anal. calcd. for $C_{24}H_{42}Si_2Mg$: C,

70.1; H, 10.3. Found: C, 70.0; H, 10.6. The E.I. mass spectrum showed a molecular ion at m/e= 411 amu. The parent ion isotopic cluster was simulated: (calcd. %, observd. %): 409 (0, 1), 410 (100, 100), 411 (50, 51), 412 (31, 33), 413 (10, 10), 414 (3, 3).

[1,2,4-$(Me_3Si)_3C_5H_2$]Na. Tris(trimethylsilyl)cyclopentadiene (13.18 g, 4.67 mmol) was added to a suspension of sodium amide[65] in tetrahydrofuran (70 mL). The mixture was heated to 50 °C and stirred at this temperature for 14 hours, ammonia evolved and the color of the tetrahydrofuran solution changed from yellow to red-brown. The reaction mixture was centrifuged and the red-brown supernatant was taken to dryness. Prolonged exposure to dynamic vacuum at room temperature (5 h) was necessary to ensure complete removal of coordinating solvents. The off-white solid was washed with pentane (2 x 200 mL) and exposed to dynamic vacuum for 3 h yielding a colorless powder (12.01 g, 3.95 mmol, 84.1 %). ^{1}H NMR (C_5D_5N, RT, 400 MHz): 7.29 ppm (2H, s, ring-C*H*), 0.50 ppm (18H, s, Si(CH_3)$_3$), 0.31 ppm (9H, s, Si(CH_3)$_3$).

[1,2,4-$(Me_3C)_3C_5H_2$]Na. [1,2,4-$(Me_3C)_3C_5H_2$]Na was synthesized from 1,2,4-$(Me_3C)_3C_5H_3$ [66] and $NaNH_2$ according to a procedure similar to that used to prepare [1,2,4-$(Me_3C)_3C_5H_2$]Na yielding a colorless powder in 87 % yield.

Manganocenes.

[$(Me_3C)C_5H_4]_2$Mn. A mixture of [$(Me_3C)C_5H_4]_2$Mg (8.1 g, 30.4 mmol) and $MnBr_2$ (6.54 g, 30.5 mmol) was heated slowly until all the magnesocene was molten at about 100 °C. The color of this inhomogeneous mixture change to red-brown. The mixture was cooled to room temperature and tetrahydrofuran (20 mL) was added. The red solution was heated to 50 °C overnight; the mixture was cooled to room temperature and the solvent was removed under reduced pressure. The orange-red residue was extracted with toluene (100 mL). Removal of the solvent and sublimation of the orange-yellow residue at 55-60 °C in diffusion pump vacuum, yielded large red crystals up to several millimeters in diameter, but leaving a reasonable quantity of a yellow-white residue behind. The red crystals were re-sublimed (40-50 °C, diffusion pump vacuum) to yield 3.8 g (12.8 mmol, 42 %). M.p. 59-60 °C (rev.); during the melting process and subsequent heating the color of the melt changed from

red to yellow-orange. The compound was stable to at least 310 °C without decomposition. Furthermore, the liquid was found to form supercooled liquids solidifying only after freezing in liquid nitrogen. ^{1}H NMR (C_6D_6, RT): 12.7 ppm ($\nu_{1/2}$ = 3100 Hz). The absence of unreacted $[(Me_3C)C_5H_4]_2Mg$ was verified by EI mass and ^{1}H NMR spectra. The E.I. mass spectrum showed a molecular ion at m/e= 297 amu. The parent ion isotopic cluster was simulated: (calcd. %, observd. %): 297 (100, 100), 298 (21, 20), 209 (2, 3). $[(Me_3C)C_5H_4]_2Mn$ has been reported previously by another synthetic route.[19]

The yellow-white residue from the first sublimation was extracted with hot toluene (60 mL), concentrated to ca. 40 mL and slowly cooled to –25 °C. Light yellow-green crystals were obtained in 18 % yield (5.35 mmol, 2.2 g) and showed to be $[(Me_3C)C_5H_4]_2Mg(thf)_2$. ^{1}H NMR ($C_6D_6$, RT): δ 6.32-6.26 ppm (m, AA'BB', $H_{2,2'}$ and $H_{3.3'}$, 8H, ring-C*H*), 3.65 (m, α-CH of THF, 8H), 1.52 (s, CMe_3, 18H), 1.27 (m, β-CH of THF, 8H).

$[(Me_3Si)C_5H_4]_2Mn$. $[(Me_3Si)C_5H_4]_2Mn$[19] was synthesized by reaction of potassium trimethylsilylcyclopentadienide (7.7 g, 0.044 mol) and $MnBr_2$ (4.69 g, 0.022 mol) in boiling tetrahydrofuran (100 mL) overnight. The light brown suspension was taken to dryness, and the residue extracted with pentane (150 mL). Filtration, concentration of the pentane extracts to 25 mL and slow cooling to –80 °C yielded yellow crystals melting upon warming to room temperature. The resulting yellow liquid was distilled, for further purification, in diffusion pump vacuum (b.p. 92-93 °C) (3.4 g, 9.6 mmol, 44 %). ^{1}H-NMR (C_6D_6, RT): 13.0 ppm ($\nu_{1/2}$ = 524 Hz).

$[1,3\text{-}(Me_3C)_2C_5H_3]_2Mn$. To a mixture of $[1,3\text{-}(Me_3C)_2C_5H_3]_2Mg$ (2.6 g, 6.8 mmol) and $MnI_2(thf)_2$ (3.1 g, 6.8 mmol) tetrahydrofuran (50 mL) was added. The reaction mixture turned orange-red and a colorless precipitate was formed. After stirring for 24 h at room temperature the solvent was removed under reduced pressure and the residual orange powder was extracted with pentane (50 mL). The red solution was filtered, concentrated and slowly cooled to –20 °C. Two crops of orange-red crystals were collected and re-crystallized from pentane yielding 1.9 g (68 %) of the pure manganocene. M.p. 145-146 °C (rev.). Sublimation: 55-60 °C (diffusion pump vacuum). ^{1}H NMR (C_6D_6, RT): 14.5 ppm ($\nu_{1/2}$ = 2700 Hz). IR (Nujol mull; CsI windows; cm^{-1}): 1293s, 1250s, 1230w, 1197s, 1162m, 1083w, 1048w, 1040m,

1020m, 930m, 920m, 910m, 838s, 800s, 737m, 685m, 655m, 640m, 615w, 604w, 507m, 475br w, 405w, 325w, 300w. Anal. calcd. for $C_{26}H_{42}Mn$: C, 76.25; H, 10.34. Found: C, 75.91; H, 10.43. The E.I. mass spectrum showed a molecular ion at m/e= 409 amu. The parent ion isotopic cluster was simulated: (calcd. %, observd. %): 409 (100, 100), 410 (40, 38), 411 (4, 5)

[1,3-$(Me_3Si)_2C_5H_3]_2Mn$. To a mixture of [1,3-$(Me_3Si)_2C_5H_3]_2Mg$ (3.9 g, 8.8 mmol) and $MnI_2(thf)_2$ (4.0 g, 8.8 mmol) tetrahydrofuran (75 mL) was added and a colorless precipitate formed immediately. The reaction was stirred overnight and the precipitate was allowed to settle. The pale yellow solution was filtered and the filtrate was taken to dryness. The yellow residue was extracted with pentane (30 mL) and filtered. The volume was reduced to 15 mL and the solution was slowly cooled to –80 °C. Light yellow crystals formed over a period of 10 days (2.4 g, 58 %). Alternatively, the product may be purified by sublimation (50-55 °C, diffusion pump vacuum). M.p. 90-91 °C (rev.). ^{1}H NMR (C_6D_6, RT): 11.8 ppm ($\nu_{1/2}$ = 980 Hz). IR (Nujol mull; CsI windows; cm^{-1}): 1293s, 1250s, 1230w, 1197s, 1162m, 1083w, 1048w, 1040m, 1020m, 930m, 920m, 910m, 838s, 800s, 737m, 685m, 655m, 640m, 615w, 604w, 507m, 475br.w, 405w, 325w, 300w. Anal. calcd. for $C_{22}H_{42}Si_4Mn$: C, 55.76; H, 8.93. Found: C, 55.85; H, 8.95. The E.I. mass spectrum showed a molecular ion at m/e= 473 amu. The parent ion isotopic cluster was simulated: (calcd. %, observd. %): 473 (100, 100), 474 (45, 46), 475 (23, 23), 476 (7, 6), 477 (2, 2).

[(3-Me_3C)(1-Me_3Si)$C_5H_3]_2Mn$. To a mixture of [(3-Me_3C)(1-Me_3Si)$C_5H_3]_2Mg$ (2.6 g, 6.8 mmol) and $MnI_2(thf)_2$ (3.1 g, 6.8 mmol) tetrahydrofuran (100 mL) was added.. The reaction mixture turned orange and a colorless precipitate was formed. After stirring for 2 h at room temperature the solvent was removed under reduced pressure and the orange residue extracted with pentane (50 mL). The solution was filtered, concentrated to ca. 30 ml and slowly cooled to – 80 °C. Small and thin orange needles formed after 2 days at – 80 °C. The crystals were dissolved in pentane and re-crystallized (1.9 g, 68 %). The compound sublimed at 50-60 °C in diffusion pump vacuum. M.p. 106-107 °C (rev.). ^{1}H NMR (C_6D_6, RT): 19.9 ppm (18 H, $\nu_{1/2}$ = 2500 Hz), 12.3 ppm (18 H, $\nu_{1/2}$ = 1750 Hz). IR (Nujol mull; CsI windows; cm^{-1}): 1325m, 1287m, 1250br s, 1200m, 1170br.s., 1075s, 1045s, 1020w, 935m, 915s,

825br.s, 750br.s, 687m, 674m, 628s, 480m, 450w, 423s, 385br.s, 333m, 290m. Anal. calcd. for $C_{24}H_{42}Si_2Mn$: C, 65.26; H, 9.58. Found: C, 64.88; H, 9.69. The E.I. mass spectrum showed a molecular ion at m/e= 441 amu. The parent ion isotopic cluster was simulated: (calcd. %, observd. %): 441 (100, 100), 442 (37, 37), 443 (13, 13).

Single crystals suitable for a X-ray structure investigation could not be obtained neither by crystallization nor sublimation. The attempted separation of the diastereomeric mixture by slow sublimation in a sealed ampoule at 50 °C over periods of weeks yielded layered crystalline material that was not suitable for a X-ray diffraction experiment.

[1,2,4-$(Me_3C)_3C_5H_2]_2Mn$. $MnCl_2$ (2.00 g, 15.89 mmol) was suspended in tetrahydrofuran (50 mL) and sodium 1,2,4-tri-tert-butylcyclopentadienide (8.14 g, 31.8 mmol) dissolved in tetrahydrofuran (100 mL) was added. After the addition was complete a yellow solution had formed that was heated under reflux for 14 h. The solvent was removed under dynamic vacuum and the yellow-brown residue was extracted with pentane (200 mL). The pentane extract was concentrated to 50 mL and slowly cooled to –20 °C. Two crops of light yellow crystals were obtained in 5.51 g overall yield (10.6 mmol, 66 %). The compound sublimed at 90-95 °C in diffusion pump vacuum. M.p. 308-309 °C (rev.). ^1H NMR (C_6D_6, RT): 14.65 ppm ($\nu_{1/2}$ = 2807 Hz). IR (Nujol mull; CsI windows; cm^{-1}): 3115w, 1580w, 1360s, 1265m, 1245s, 1205m, 1150m, 1100br.m, 1025m, 1007m, 962w, 925w, 821sh.s, 812s, 680m, 545w, 448w, 410w, 380w, 280w. Anal. calcd. for $C_{34}H_{58}Mn$: C, 78.27; H, 11.20. Found: C, 78.06; H, 11.18. The E.I. mass spectrum showed a molecular ion at m/e= 521 amu. The parent ion isotopic cluster was simulated: (calcd. %, observd. %): 521 (100, 100), 522 (28, 28), 523 (5, 5). The synthesis of this compound has been reported recently,[50] but some of the stated properties differ from those obtained in this work. $[1,2,4\text{-}(Me_3C)_3C_5H_2]_2Mn$ does not react with bipy, Li(neopentyl), H_2 (up to 16 atm) or CO (up to 13 atm).

[1,2,4-$(Me_3Si)_3C_5H_2]_2Mn$. To a mixture of sodium tris(trimethylsilyl)cyclopentadienide (5.93 g, 19.5 mmol) and $MnI_2(thf)_2$ (4.42 g, 9.75 mmol) tetrahydrofuran (150 mL) was added. A colorless precipitate formed immediately. The solution was heated to reflux for 2 hours, then cooled to room temperature.

The solvent was removed under dynamic vacuum and the residue extracted with pentane (150 mL). The pentane extract was concentrated to 20 mL and slowly cooled to –80 °C yielding ivory-colored crystals (3.05 g, 4.94 mmol, 51 %). Further purification was performed by sublimation in diffusion pump vacuum (70-80 °C). M.p. 286-288 °C (rev.). ^{1}H NMR (C_6D_6, RT): two very broad signals, one of which overlapped with C_6D_6: ~ 10 ppm ($\nu_{1/2}$ ~ 1050 Hz) and ~ 7 ppm ($\nu_{1/2}$ ~ 750 Hz). IR (Nujol mull; CsI windows; cm^{-1}): 3060vw, 1335vw, 1248s, 1135w, 1088s, 1002m, 940m, 835vs, 752s, 688w, 738m, 728m, 504w, 430w, 395w, 378w, 340br.w. Anal. calcd. for $C_{28}H_{56}Si_6Mn$: C, 54.46; H, 9.40. Found: C, 54.17; H, 9.43. The E.I. mass spectrum showed a molecular ion at m/e= 617 amu. The parent ion isotopic cluster was simulated: (calcd. %, observd. %): 617 (100, 100), 618 (62, 61), 619 (39, 40), 620 (15, 15), 621 (1, 2).

Significant amounts of decomposition were observed on reaction with $H_2(D_2)$ (10 atm) or CO (16 atm). No deuterium incorporation into the cyclopentadienyl ring was detected by ^{2}H NMR spectroscopy. The compound decomposed completely under an atmosphere of H_2 (D_2) over a period of 4 days to $(Me_3Si)_3C_5H_3$ and an insoluble brown residue.

Attempted Synthesis of {[1,3-$(Me_3C)_2C_5H_3$][1,3-$(Me_3Si)_2C_5H_3$]Mn}. The missing link within the series of tetrasubstituted manganocenes was the heteroleptic representative, {[1,3-$(Me_3C)_2C_5H_3$][1,3-$(Me_3Si)_2C_5H_3$]Mn}. In contrast to [1,3-$(Me_3C)(Me_3Si)C_5H_3]_2$Mn, this isomer does not form a mixture of diasteromers. However, the synthesis of such a molecule was not straightforward: A solution synthesis was hampered by the fact that high-spin manganocenes with labile cyclopentadienyl ligands were prone to ligand redistribution reactions, which were furthermore driven by the formation of the enthalpy favored, low-spin [1,3-$(Me_3C)_2C_5H_3]_2$Mn species. However, in some cases metathesis reactions in molten solutions were employed successfully to synthesis labile organometallic species, e.g. $(C_5H_5)Mg(CH_2CMe_3)$.[77] Accordingly, a 1:1 mixture of [1,3-$(Me_3C)_2C_5H_3]_2$Mn and [1,3-$(Me_3Si)_2C_5H_3]_2$Mn formed an eutectic melt with a melting range 80-83 °C. Heating the sample to 150 °C over a period of 1 month set up a mixture of hetero- and homoleptic compounds as determined by electron-impact mass spectrometry (EI-MS) (m.p. 74-77 °C). Determining the quantitative composition

of the mixture was nearly impossible considering the significant line broadening in the ^{1}H NMR spectra, which precluded an accurate integration. Alternatively UV-vis spectra were hard to deconvolute into the three contributors without pure {[1,3-$(Me_3C)_2C_5H_3$][1,3-$(Me_3Si)_2C_5H_3$]Mn} available. The qualitative composition did not change upon heating for a additional month to about 200 °C (m.p. 68-70 °C) as determined by EI-MS. The reaction mixture was sublimed in order to achieve some separation (40-50 °C in diffusion pump vacuum). At this point it was of interest to get a qualitative insight into the magnetism of the mixture (see Supporting Information for details). As shown in Figure S27, the magnetic moment was clearly different from the one obtained for the homoleptic species. Interestingly, the magnetism resembled the behavior of [1,3-$(Me_3C)(Me_3Si)C_5H_3]_2$Mn the high-spin population stayed constant to ~ 120 K, then gradually increased - more or less linearly - with T up to 300 K, but without reaching a saturation value. Unfortunately, the relative proportions of the different species were not available, and therefore it was impossible to determine the contribution of "pure" {[1,3-$(Me_3C)_2C_5H_3$][1,3-$(Me_3Si)_2C_5H_3$]Mn} in this mixture. However, the close qualitative relation to [1,3-$(Me_3C)(Me_3Si)C_5H_3]_2$Mn suggested that both molecules were electronically rather similar. At low temperature the ground state was a mixture of a constant population of high- and low-spin molecules, but from 120 K the low-spin molecules gradually converted into high-spin molecules. This proceeded in the mixture more gradually than in [1,3-$(Me_3C)(Me_3Si)C_5H_3]_2$Mn.

Acknowledgments

This work was supported by the Director, Office of Science, Office of Basic Energy Sciences (OBES), of the U.S. Department of Energy under Contract No. DE-AC02-05CH11231. X-ray absorption data were collected at the Stanford Synchrotron Radiation Laboratory, a national user facility operated by Stanford University on behalf of the DOE/OBES. We thank Dr Fred Hollander (at CHEXRAY, the U.C. Berkeley X-ray diffraction facility) for assistance with the crystallography, the German Academic

Exchange Service (DAAD) for a fellowship (M.D.W.) and Wayne W. Lukens for discussions and assistance with the EPR studies.

Supporting Information Available

Crystallographic data, labeling diagrams, tables giving atomic positions, anisotropic thermal parameters, bond distances, bond angles, torsion angels, least square planes for each structure, solid state magnetism data of $(C_5Me_5)_2Mn$, $[(Me_3E)_nC_5H_{5-n})]_2Mn$ (E= C, Si; n= 1, 2, 3), packing diagrams for $[(Me_3C)_2C_5H_3)]_2Mn$ and $[(Me_3Si)_2C_5H_3)]_2Mn$, HS → LS relaxation for $[1,3\text{-}(Me_3C)(Me_3Si)C_5H_3]_2Mn$ after thermal trapping, EPR spectra of $[(Me_3Si)_2C_5H_3]_2Mn$, $[(Me_3C)_2C_5H_3]_2Mn$ and $[(1,3\text{-}Me_3C)(Me_3Si)C_5H_3]_2Mn$, normalized mole fraction vs. T plot for high-spin, low-spin equilibrium of $[(Me_3C)C_5H_4]_2Mn$ and $[1,3\text{-}(Me_3C)(Me_3Si)C_5H_3]_2Mn$, variable temperature Mn K edge XANES and EXAFS studies for $[(Me_3C)_2C_5H_3]_2Mn$, temperature dependence of the UV-vis absorption at 269 nm for $[1,3\text{-}(Me_3Si)_2C_5H_3]_2Mn$ and at 430 nm for $[(1,3\text{-}Me_3C)(Me_3Si)C_5H_3]_2Mn$. This material is available free of charge via the Internet at http://pubs.acs.org. Structure factor tables are available from the authors. Crystallographic data were also deposited with Cambridge Crystallographic Data Centre. Copies of the data (CCDC 700163-700167) can be obtained free of charge via http://www.ccdc.cam.ac.uk/data_request/cif by e-mailing data_request@ccdc.cam.ac.uk, or by contacting The Cambridge Crystallographic Data Centre, 12, Union Road, Cambridge CB 1EZ, UK; fax +44 1223 336033.

References

[1] Wilkinson, G.; Cotton, F. A., *Chem. Ind. (London)* **1954,** *11*, 307-308.

[2] Wilkinson, G.; Cotton, F. A., *Prog. Inorg. Chem.* **1959,** *1*, 1.

[3] Fischer, E. O.; Jira, R., *Z. Naturforsch.* **1954,** *9B*, 618-619.

[4] Grebenik, P.; Grinter, R.; Perutz, R. N., *Chem. Soc. Rev.* **1988,** *17*, 453-490.

[5] Haaland, A., *Top. Curr. Chem.* **1975,** *53*, 1-23.

[6] Haaland, A., *Inorg. Nucl. Chem. Lett.* **1979,** *15*, 267-269.

[7] Wilkinson, G.; Cotton, F. A.; Birmingham, J. M., *J. Inorg. Nucl. Chem.* **1956,** *2*, 95-113.

[8] Almenningen, A.; Haaland, A.; Samdal, S., *J. Organomet. Chem.* **1978,** *149*, 219-229.

[9] Evans, S.; Green, M. L. H.; Jewitt, B.; King, G. H.; Orchard, A. F., *J. Chem. Soc., Faraday II* **1974,** *70*, 356-376.

[10] [(a)] Green, J. C.; Decleva, P., *Coord. Chem. Rev.* **2005,** *249*, 209. [(b)] Green, J. C., *Faraday Discuss.* **2003**, *124*, 453-455. [(c)] Green, J. C.; Burney, C., *Polyhedron* **2004**, *23*, 2915-2919.

[11] Ammeter, J. H.; Bucher, R.; Oswald, N., *J. Am. Chem. Soc.* **1974,** *96*, 7833-7835.

[12] Ammeter, J. H., *J. Magn. Reson.* **1978,** *30*, 299-325.

[13] Ammeter, J. H.; Zoller, L.; Bachmann, J.; Baltzer, P.; Gamp, E.; Bucher, R.; Deiss, E., *Helv. Chim. Acta* **1981,** *64*, 1063-1082.

[14] Switzer, M. E.; Wang, R.; Rettig, M. F.; Maki, A. H., *J. Am. Chem. Soc.* **1974,** *96*, 7669-7674.

[15] Cauletti, C.; Green, J. C.; Kelley, M. R.; Powell, P.; Tilborg, J. V.; Robbins, J.; Smart, J., *J. Electron Spectrosc. Relat. Phenom.* **1980,** *19*, 327-353.

[16] Freyberg, D. P.; Robbins, J. L.; Raymond, K. N.; Smart, J. C., *J. Am. Chem. Soc.* **1979,** *101*, 892-897.

[17] Smart, J. C.; Robbins, J. L., *J. Am. Chem. Soc.* **1978,** *100*, 3936-3937.

[18] Bünder, W.; Weiss, E., *Z. Naturforsch.* **1978,** *33b*, 1237-1238.

[19] Hebendanz, N.; Köhler, F. H.; Müller, G.; Riede, J., *J. Am. Chem. Soc.* **1986,** *108*, 3281-3289.

[20] Gardiner, M. G.; Raston, C. L.; Kennard, C. H. L., *Organometallics* **1991,** *10*, 3680-3686.

[21] For the coordination number 6 the ionic radii are: Mn^{2+} (HS)= 0.83 Å, Mn^{2+} (LS)= 0.67 Å and Mg^{2+}= 0.72 Å (Shannon, R. D., *Acta Cryst. A* **1976,** *A32*, 751-767).

[22] The effective magnetic moment is directly related to the spin and orbit quantum numbers as follows: $\mu_{eff} = \sqrt{4S(S+1)+L(L+1)}$. For ions with A and E ground state terms, the magnetic properties can be assigned as predominantly spin in nature since most of the orbital angular moment has been quenched. Orbital quenching is nearly complete for ions with A_{1g} ground terms and, as a result, the g values are very close to the free spin value of 2.0, and the zero field splitting of the spin degeneracies is usually small. Partial quenching is apparent in the other ions with A and E ground state terms, resulting in g value anisotropies, deviation of the moment from the spin only value, and larger zero field splittings of the spin multiplets. For manganocenes, the high-spin isomer with an $^6A_{1g}$ ground term exhibits a magnetic moment of $\mu_{eff} = 2\sqrt{2.5\times3.5}$ = 5.92 μ_B, since L= 0.

[23] Figgis, B. N., *Introduction to Ligand Fields*.; J. Wiley & Sons: New York, 1966; Chapter 10.

[24] Hays, M. L.; Burkey, D. J.; Overby, J. S.; Hanusa, T. P.; Sellers, S. P.; Yee, G. T.; Young, V. G., *Organometallics* **1998,** *17*, 5521-5527.

[25] Robbins, J. L.; Edelstein, N. M.; Cooper, S. R.; Smart, J. C., *J. Am. Chem. Soc.* **1979,** *101*, 3853-3857.

[26] Kahn, O., *Molecular Magnetism*.; VCH: New York, 1993.

[27] Spiering, H.; Meissner, E.; Köppen, H.; Müller, E. W.; Gütlich, P., *Chem. Phys.* **1982,** *68*, 65-71.

[28] Adler, P.; Wiehl, L.; Meissner, E.; Köhler, C. P.; Spiering, H.; Gütlich, P., *J. Phys. Chem. Sol.* **1987,** *48*, 517-525.

[29] Guionneau, P.; Létard, J.-F.; Yufit, D. S.; Chasseau, D.; Bravic, G.; Goeta, A. E.; Howard, J. A. K.; Kahn, O., *J. Mater. Chem.* **1999,** *9*, 985-994.

[30] Augart, N.; Boese, R.; Schmid, G., *Z. Anorg. Allgem. Chem.* **1991,** *595*, 27-34.

[31] Létard, J.-F.; Capes, L.; Chastanet, G.; Moliner, N.; Létard, S.; Real, J.-A.; Kahn, O., *Chem. Phys. Lett.* **1999,** *313*, 115-120.

[32] Buchen, T.; Gütlich, P.; Sugiyarto, K. H.; Goodwin, H. A., *Chem. Eur. J.* **1996,** *2*, 1134-1138.

[33] Buchen, T.; Gütlich, P.; Goodwin, H. A., *Inorg. Chem.* **1994,** *33*, 4573-4576.

[34] Hauser, A., *Chem. Phys. Lett.* **1992,** *192*, 65-70.

[35] Hauser, A., *Comments Inorg. Chem.* **1995,** *17*, 17-40.

[36] Marchivie, M.; Guionneau, P.; Létard, J.-F.; Chasseau, D.; Howard, J. A. K., *J. Phys. Chem. Solids* **2004,** *65*, 17-23.

[37] Roubeau, O.; deVos, M.; Stassen, A. F.; Burriel, R.; Haasnoot, J. G.; Reedijk, J., *J. Phys. Chem. Solids* **2003,** *64*, 1003-1013.

[38] Ritter, G.; König, E.; Irler, W.; Goodwin, H. A., *Inorg. Chem.* **1978,** *17*, 224-228.

[39] Yu, Z.; Liu, K.; Tao, J. Q.; Zhong, Z. J.; You, X. Z.; Siu, G. G., *Appl. Phys. Lett.* **1999,** *74*, 4029-4031.

[40] Roubeau, O.; Stassen, A. F.; Gramage, I. F.; Codjovi, E.; Linarès, J.; Varret, F.; Haasnoot, J. G.; Reedijk, J., *Polyhedron* **2001,** *20*, 1709-1716.

[41] [(a)] Gütlich, P.; van Koningsbruggen, P. J.; Renz, F., *Struct. Bonding* **2004,** *107*, 24-75, and references therein.; [(b)] Gütlich, P.; Goodwin, H.A., *Top. Curr. Chem.* **2004**, *233*, 1-47; and references therein.

[42] Okamoto, K.; Nagai, K.; Miyawaki, J.; Kondoh, H.; Ohta, T., *Chem. Phys. Lett.* **2003,** *371*, 707-712.

[43] Thuery, P.; Zarembowitch, J.; Michalowicz, A.; Kahn, O., *Inorg. Chem.* **1987,** *26*, 851-5.

[44] Boca, M.; Vrbova, M.; Werner, R.; Haase, W., *Chem. Phys. Lett.* **2000,** *328*, 188-196.

[45] Paulsen, H.; Grunsteudel, H.; Meyer-Klaucke, W.; Gerdan, M.; Grunsteudel, H. F.; Chumakov, A. I.; Ruffer, R.; Winkler, H.; Toftlund, H.; Trautwein, A. X., *Eur. Phys. J. B* **2001,** *23*, 463-472.

[46] Rudd, D. J.; Goldsmith, C. R.; Cole, A. P.; Stack, T. D. P.; Hodgson, K. O.; Hedman, B., *Inorg. Chem.* **2005,** *44*, 1221-1229.

[47] Hannay, C.; Hubin-Franskin, M.-J.; Grandjean, F.; Briois, V.; Itie, J. P.; Polian, A.; Trofimenko, S.; Long, G. J., *Inorg. Chem.* **1997,** *36*, 5580-5588.

[48] Booth, C. H.; Bridges, F.; Kwei, G. H.; Lawrence, J. M.; Cornelius, A. L.; Neumeier, J. J., *Phys. Rev. B* **1998,** *57*, 10440-10454.

[49] The X-ray absorption near-edge structure (XANES) region is consistent with the interpretation that the electronic state is best described as a mixture of the HS and LS configurations in the crossover region near 350 K, see Supporting Information, Figure S28 for further details.

[50] Sitzmann, H.; Schär, M.; Dormann, E.; Kelemen, M., *Z. Allgem. Anorg. Chem.* **1997,** *623*, 1609-1613.

[51] Van Zee, R. J.; Brown, C. M.; Weltner, W., *Chem. Phys. Lett.* **1979,** *64*, 325-328.

[52] DeVore, T. C.; Van Zee, R. J.; Weltner, W., *J. Chem. Phys.* **1978,** *68*, 3522-3527.

[53] Weltner, W., *Magnetic Atoms and Molecules*.; Dover Publications: New York, 1983.

[54] The magnetic moment of the low-spin isomer can be calculated based on EPR studies using the following equation: $\mu_{LS} = \left\{\frac{1}{3}(g_{\perp}{}^2 + 2g_{\parallel}{}^2)(S)(S+1)\right\}^{1/2}$.

[55] Kira, M.; Watanabe, M.; Sakurai, H., *J. Am. Chem. Soc.* **1980,** *102*, 5202-5207.

[56] Barker, P. J.; Davies, A. G.; Tse, M., *J. Chem. Soc. Perkin II* **1980**, 941-948.

[57] Lukens, W. W.; Matsunaga, P. T.; Andersen, R. A., *Organometallics* **1998,** *17*, 5240.

[58] Walter, M. D.; Schultz, M.; Andersen, R. A., *New J. Chem.* **2006,** *30*, 238-246.

[59] Walter, M. D.; Berg, D. J.; Andersen, R. A., *Organometallics* **2006,** *25*, 3228-3237.

[60] O'Connor, C. J., *Prog. Inorg. Chem.* **1982,** *29*, 203-285.

[61] Riemscheider, R.; Reisch, A.; Horak, H., *Monatsh. Chem.* **1960,** *91*, 805-811.

[62] Duff, A. W.; Hitchcock, P. B.; Lappert, M. F.; Taylor, R. G.; Segal, J. A., *J. Organomet. Chem.* **1985,** *293*, 271-283.

[63] Sofield, C. D.; Andersen, R. A., *J. Organomet. Chem.* **1995,** *501*, 271-276.

[64] Lukens, W. W.; Beshouri, S. M.; Blosch, L. L.; Stuart, A. C.; Andersen, R. A., *Organometallics* **1999,** *18*, 1235-1246.

[65] Greenlee, K. W.; Henne, A. L., *Inorg. Synth.* **1946,** *2*, 128-135.

[66] Dehmlow, E. V.; Bollmann, C., *Z. Naturforsch.* **1993,** *48b*, 457-460.

[67] Keski-Rahkonen, O.; Krausse, M. O., *At. Data Nucl. Data Tables* **1974,** *14*, 139-146.

[68] Ankudinov, A. L.; Rehr, J. J., *Theory. Phys. Rev. B* **1997,** *56*, R1712-R1716.

[69] Real Space X-ray Absorption Package. http://lise.lbl.gov/RSXAP/.

[70] Li, G. G.; Bridges, F.; Booth, C. H., *Phys. Rev. B* **1995,** *52*, 6332-6348.

[71] Brennan, J. G. Ph.D. Thesis. University of California, Berkeley, 1985.

[72] Kraihanzel, C. S.; Losee, M. L., *J. Am. Chem. Soc.* **1968,** *90*, 4701-4705.

[73] Abel, E. W.; Moorhouse, S., *J. Organomet. Chem.* **1971,** *29*, 227-232.

[74] Venier, C. G.; Casserly, E. W., *J. Am. Chem. Soc.* **1990,** *112*, 2808-2809.

[75] Okuda, J., *Chem. Ber.* **1989,** *122*, 1075-1078.

[76] Jutzi, P.; Sauer, R., *J. Organomet. Chem.* **1973,** *50*, C29-C30.

[77] Andersen, R. A.; Blom, R.; Haaland, A.; Schilling, B. E. R.; Volden, H. V., *Acta Chem. Scand. A* **1985,** *39*, 563-569.

For Table of Contents (TOC) Only.

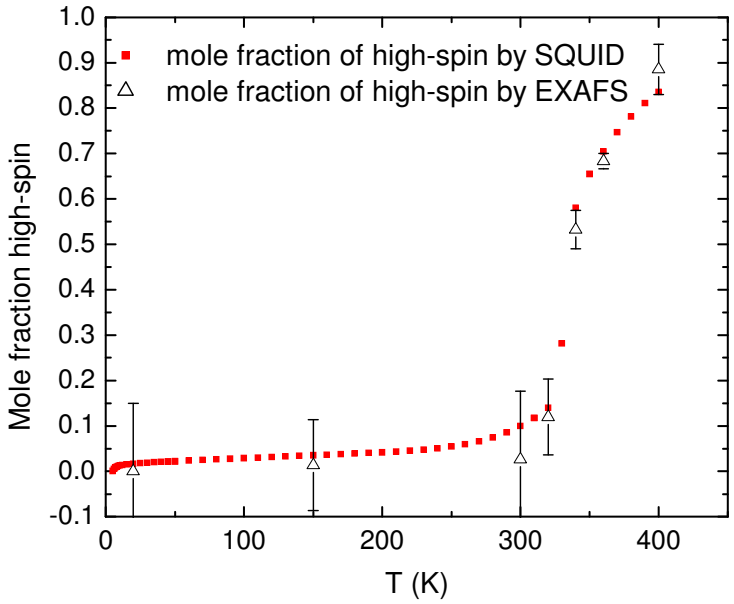

Interpretation of variable temperature EXAFS data give a molecular level of understanding to magnetic susceptibility curves in spin-equilibrium manganocenes; $[1,3\text{-}(Me_3C)_2C_5H_3]_2Mn$.